Polanen GT: Seismic Hazard Analysis

Project: 1900011

April, 2022

Polanen GT: Seismic Hazard Analysis

Authors
[redacted]

Reviewed by
[redacted]

Release authorised by:
[redacted]

Prepared for
HVC
Baanhoekweg 38
3313 LA Dordrecht
Nederland

Prepared by
PanTerra Geoconsultants B.V.
Weversbaan 1-3
2352 BZ Leiderdorp
The Netherlands
T +31 (0)71 581 35 05
F +31 (0)71 301 08 02
info@panterra.nl

1 Nederlandse samenvatting

Dit rapport geeft een Level-2 (locatie-specifieke) Seismic Hazard Assessment (SHA) voor het Polanen aardwarmteproject van HVC. De score van de Polanen SHA Level-1 Quick-Scan (Q-CON/IF technology, 2016) werd eerder vastgesteld op 0.31 door (PanTerra, 2020b). Deze score betekent dat er een laag seismisch risico is. Vanwege de oriëntatie van het spanningsveld en het feit dat het doublet wordt geplaatst in een gebied dat afgescheiden is door breuken zijn de risico's mogelijk hoger. Om de risico's grondiger te analyseren is een locatie-specifieke SHA uitgevoerd voor de geothermische operatie van Polanen. Uit deze beoordeling volgt dat, voor injectie in de Delft zandsteen formatie, het seismisch risico "laag" is.

Figuur 1-1 is een kaart van de top van het Delft reservoir – gekleurd met diepte. De breuken zijn aangegeven met grijze polygonen. De meest opvallende breuken zijn de F3 en F4 breuken. Breuk F3 heeft een verzet van 0-20 m op ~625 m van de injectieput. Breuk F4 heeft een verzet van ~75 m op een afstand van ~725 m van de injectieput.

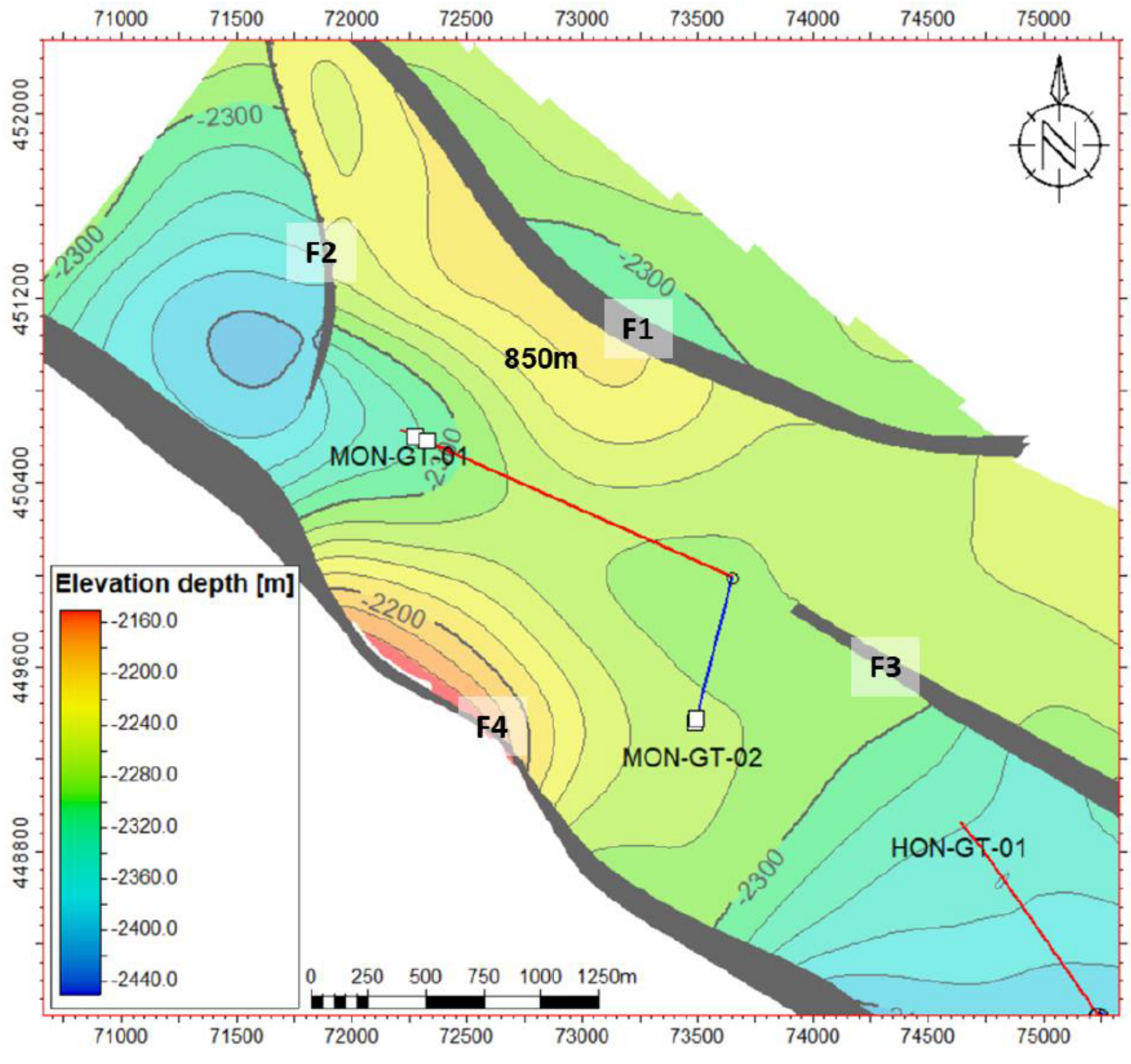

Figuur 1-1 Top Delft reservoir dieptekaart van het winningsgebied met geplande putten, penetratiepunten (witte vierkantjes) en breuklijnen (grijs, F1 tot F4).

Het Polanen aardwarmteproject heeft als doel om ~86°C water te produceren uit de Delft zandsteen formatie en om koud water met laagst mogelijke temperatuur van 35°C terug in hetzelfde reservoir te injecteren. Wanneer het geïnjecteerde water een breuk bereikt kunnen de spanningen op die breuk veranderen en in theorie leiden tot breuk reactivatie en seismische activiteit. Of een breuk mogelijk wordt geactiveerd of niet kan berekend worden door middel van een geomechanische analyse.

Het risico op breukactivatie wordt uitgedrukt in de parameter SCU (Shear Capacity Utilisation). Bij een SCU kleiner dan 1 is breukactivatie onmogelijk. Zodra deze parameter groter wordt dan 1 bestaat een kans op breukactivatie. Echter bij een SCU>1 hoeft in de praktijk geen breukactivatie op te treden. Op dit moment zijn er nog geen projecten in de operatiefase met een SCU>1 waarbij breukactivatie is waargenomen.

Een relevant fenomeen in deze studie is "arching" – wat betekent dat niet-afgekoelde delen van het reservoir het gewicht van ondiepere lagen dragen. Dit effect is het sterkst wanneer de laterale extensie van het afgekoelde gebied beperkt is. "Arching" beperkt de kans op breuk (re)activatie en het effect hiervan wordt berekend in de geomechanische modellen. Het effect van "arching" kan afnemen gedurende de levensduur van het doublet. Dit komt omdat de laterale extensie van de afgekoelde zone toeneemt naarmate er langer geïnjecteerd wordt. Hoe groter deze laterale extensie wordt, hoe minder "arching" plaatsvindt door aangrenzende niet afgekoelde reservoir zones.

De hier toegepaste workflow is recentelijk ontwikkeld door PanTerra (van den Hoek & Poessé, 2021), omdat de huidige richtlijnen van Q-CON/IF technology (2016) voor een "niveau 2" SHA geen duidelijk kader bevat hoe dit soort studies uitgevoerd moeten worden. De werkwijze bevat een geomechanische bepaling van de temperatuur van het koelere waterfront en van de thermo-mechanische effecten gedurende de termijn van de Polanen geothermische operatie.

Voor dit doel zijn twee types van geomechanische modellen gebruikt:

1. Een 2-D analytisch model dat het mechanisme weergeeft van mogelijke seismische activiteit door berekening van lokale spanningsveranderingen rond een breuk als gevolg van geothermische operaties gedurende de termijn van de geothermische operatie.

2. Een 3-D Mohr-Coulomb benadering die gebruikt wordt voor probalistische methodologie, waarbij de kans op een mogelijke seismische gebeurtenis wordt geanalyseerd.

De conclusie van deze studie is dat voor 35°C water injectie in de Delft zandsteen formatie gedurende 30 jaar het risico op breuk reactivatie van breuk F3 bij afkoeling "laag" is (n.l., 11% > 1.0 SCU). Voor breuk F4 geldt een vergelijkbaar "laag" risico (n.l., 10% > 1.0 SCU). De risico's op seismische activiteit door injectie voor het doublet MON-GT-01/02 zijn "laag".

Index of figures

Index of tables

Contents

2 Introduction

2.1 Area of interest

The Polanen doublet, owned by HVC, is situated in the municipality of Westland in the province Zuid-Holland. The doublet, consisting of producer MON-GT-01 and injector MON-GT-02, is located within the Monster 2 geothermal exploration concession (Figure 2-1). The target reservoirs are the fluvial sands of the Delft Sandstone Member, which is the main target of other doublets in this region.

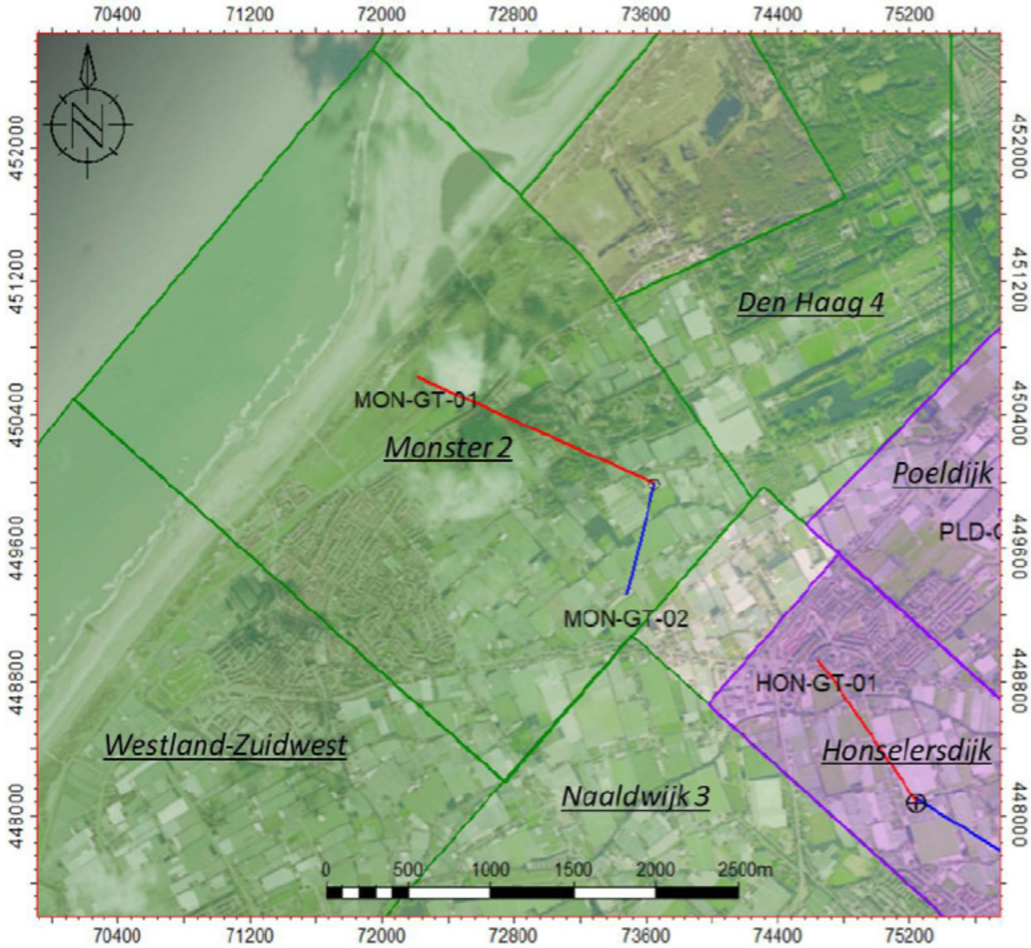

Figure 2-1 Location of planned wells with reference to geothermal licences (purple: production licence, green: exploration licence) and nearby geothermal doublets (producers in red, injectors in blue).

2.2 Guidelines for geothermal projects

A Decision tree (Figure 2-2) for carrying out a Seismic Hazard Assessement (SHA) has been made by Q-CON/IF technology (2016). This decision tree contains three risk levels, with required levels of relevant studies associated to it. In 2020, a Level 1 SHA (lowest level 'Quickscan') was carried out for Polanen as part of the production license application (PanTerra, 2020b). The resulting score from the SHA Quick-Scan was determined to be equal to 0.31 for each of the planned doublets by (PanTerra, 2020b). This is associated with low seismic risk. However, due to the orientation of the stress field and the fact that the doublet will be placed in an area separated by faults, the risks can arguably be classified higher. Therefore, an independent detailed geomechanical study (location-specific seismic hazard assessment) was performed for the geothermal operation of Polanen. This report touches upon the aspects that are involved in a Level 2 SHA. The current guidelines by IF/Q-CON only partially define the level-2 SHA and no clear framework exist about how to conduct such a study. For this reason a recently developed new SHA-methodology (van den Hoek & Poessé, 2021) was applied for Polanen.

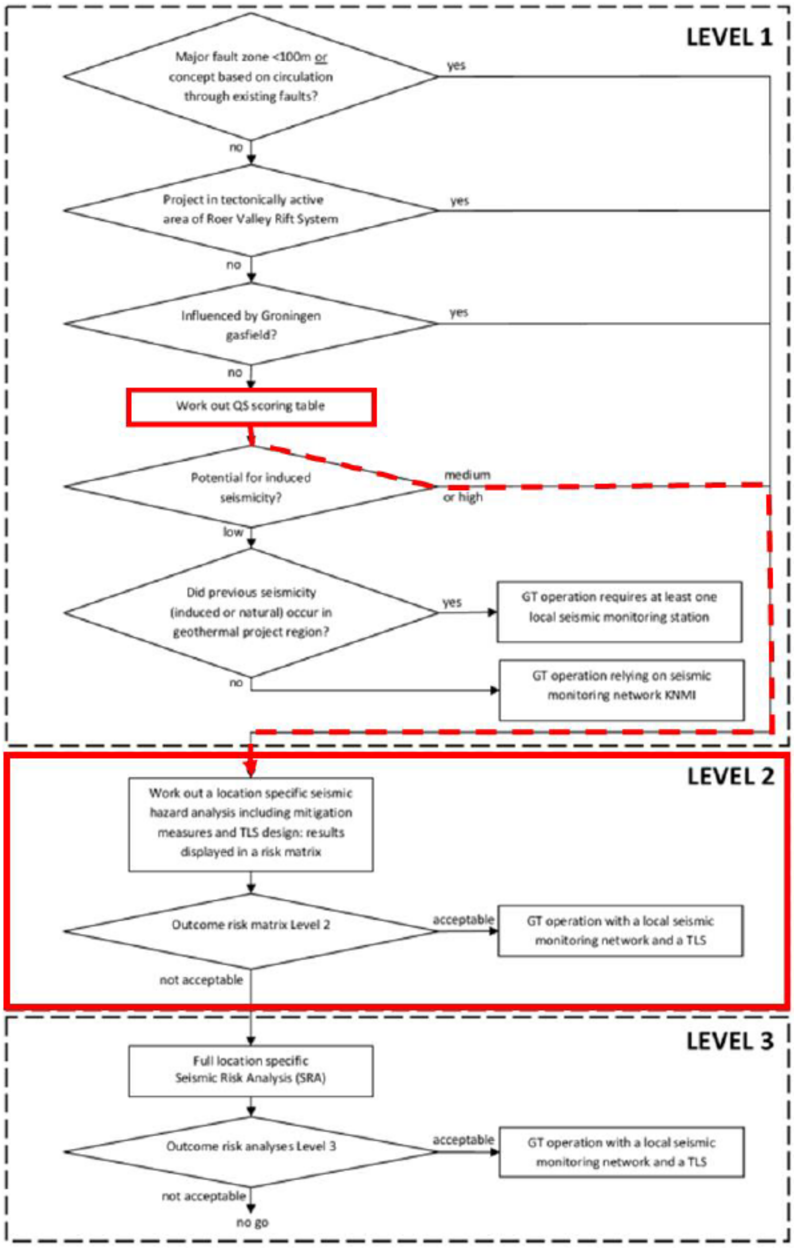

Figure 2-2 Decision tree as presented in the report by Q-CON/IF technology (2016). In this report Level 2 (red outline) is covered. TLS stands for Traffic Light System.

3 Methodology

Because currently no guidelines exist for carrying out a Level 2 Seismic Hazard Assessment (SHA), the methodology used in this study is based on the recently proposed approach by van den Hoek & Poessé (2021). Geo-mechanical models were created to understand the thermo-mechanical effects in the lifetime of the Polanen geothermal operation. Van den Hoek & Poessé (2021) used an analytical analysis to carry out a detailed study of the stress changes along nearby faults as a result of geothermal operations over the lifetime of a field. In the current study, the same approach is used. The analytical model can be considered as an exact solution to the stress concentrations induced by cooling. The focus of this study is the geomechanical effects in the Delft formation. The approach to simulate the stress changes induced by cooling is presented in some more detail in paragraph 2.1 below. The 3-D Mohr-Coulomb model uses both a deterministic and a probabilistic methodology. This methodology was presented in 2020 by Poessé & van den Hoek (2020) and is summarised in section 3.2.

At the moment no seismic events or small earthquakes have been reported as a result of geothermal operations. In future, when seismic sensors detect seismic activity, the models will need to be calibrated and predictions can be updated.

3.1 Two-dimensional analytical model to simulate stress changes induced by cooling

The analytical model was developed in-house. It is based on an elaboration of the so-called Goodier integral expression for stresses induced by changes in reservoir pressure and / or temperature, see for example Koning (1988). This results in an exact solution of the induced stress changes, and therefore comparison with finite element calculations of the same geometry should give good agreement. This is indeed what was achieved in a validation study by PanTerra that was carried out as part of the in-house model development.

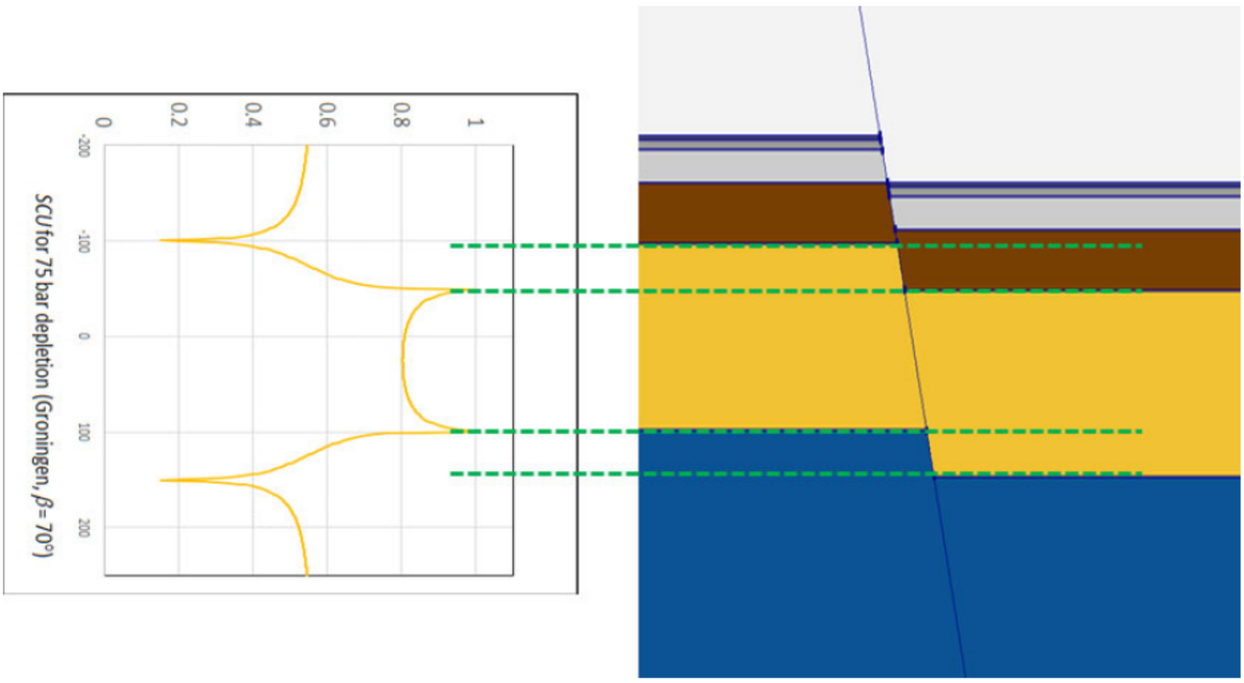

Figure 3-1 Profile of the computed "Shear Capacity Utilisation" (SCU) along the fault for a Groningen-field situation, with 75 bar reservoir depletion.

Figure 3-1 shows a typical result as computed for the example of 75 bar depletion in the Groningen field. The case of stress concentrations on the fault as a result of reservoir depletion in Groningen has been widely published, see for example Buijze et al. (2017), Poessé & van den Hoek (2020), van den Hoek and Poessé (2021), and van den Bogert (2015). Figure 3-1 shows the profile of the so-called "Shear Capacity Utilisation" (SCU) along the fault which is defined by

$$SCU \; = \div \frac{\text{Shear stress along the fault}}{\text{Maximum shear stress along the fault}} = \frac{\text{Shear stress along the fault}}{C \; + (\text{Normal stress on the fault}\;) \; \times \; \tan(\varphi)}$$

where C and φ are the cohesion and friction angle of the fault, respectively. The SCU can be viewed as a quantitative measure of how close the fault is to "failure" (activation), which is indicated by a value of SCU = 1. In Figure 3-1 it can be seen that there are shear stress concentrations, resulting in high SCU, at the top of the hanging wall reservoir (right) and the bottom of the foot wall reservoir (left). This is a well-known phenomenon that takes place along faults with nonzero offsets crossing depleting reservoirs, see again van den Bogert (2015), Poessé & van den Hoek (2020), (van den Hoek & Poessé, 2021), and TNO (2014). With progressing reservoir depletion beyond 75 bar, the SCU of the entire fault area between the top of the hanging wall (right) and bottom of the foot wall (left) becomes equal to one, which eventually could cause fault slip over this area. This potential movement along the fault does not directly imply that seismicity and small earthquakes will occur (Poessé & van den Hoek, 2020), (van den Hoek & Poessé, 2021).

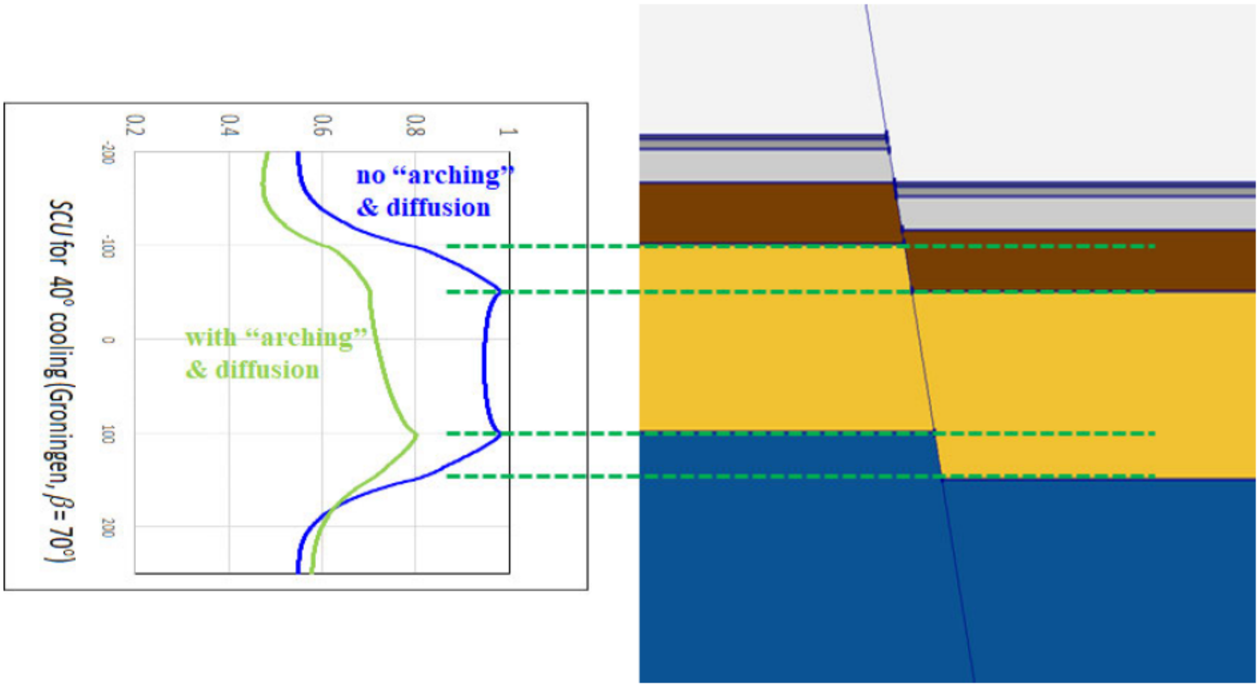

Figure 3-2 Profile of the computed "Shear Capacity Utilisation" (SCU) along the fault for a Groningen-field situation, with (hypothetical) 40°C reservoir cooling.

The effect of stress concentration along faults with nonzero offsets not only takes place as a result of reservoir depletion, but also as a result of reservoir cooling. Stress changes as an effect of reservoir cooling is illustrated Figure 3-2 for the same (Groningen) reservoir as Figure 3-1, but now for a (hypothetical) cooling by 40°C. However, an essential difference with (gas) reservoir depletion is that in this case, only a very limited part of the reservoir is cooled, even after around 30 years of operation. Moreover, as a result of thermal diffusion within the reservoir and from the cap- and base-rock, the temperature varies more smoothly and large parts of the reservoir, especially further away from the injector, cool only partially. The finite size of the (partially) cooled reservoir results in arching by the non-cooled areas of the reservoir, and therefore the SCU at the fault can be significantly lower. This is illustrated in Figure 3-2. Here, the blue curve represents a situation where the entire reservoir has been cooled, whereas the green curve represents a situation where only a few hundred meters around the injector have been (partially) cooled. As will be shown below for the Polanen cases, a cooled zone extent of a few hundred metres to a kilometer is realistic for a geothermal operation that lasts about 10-30 years.

3.2 (Probabilistic) Mohr-Coulomb modelling

The state of stress can be defined by the means the Mohr-circles and associated Mohr-Coulomb failure criterion. The Mohr-circle represents the state of stress for any given orientation in a 2D or 3D space, with as input the maximum, minimum and in case of 3D the intermediate stress. In the presence of a fault, a failure criterion can be defined by the cohesion and friction coefficient of this fault. If the state of stress in a specific orientation exceeds the failure criterion, shear slip movement may occur along the fault. The goal of the Mohr-Coulomb exercise is to know at what limit slip along the fault may occur which is a potential hazard coming from a subsurface operation.

Mohr-Coulomb only addresses the stress state at one point in space. In order to address parameter uncertainties, a probabilistic Mohr-Coulomb approach ("Mohr-Coulomb Monte-Carlo") is applied to the point along the fault where failure is most likely, i.e. the point with highest SCU. This can be considered a conservative approach because it only addresses the failure likelihood of *the "worst" point along the fault*, whereas fault slip requires failure (SCU = 1) over a larger contiguous fault area, just like in the Groningen depletion case.

The effect of local stress arching for a geothermal project is illustrated in Figure 3-2 and Figure 3-3. In the case of geothermal projects, the local higher stress concentrations along a fault can be offset by the fact that the stress perturbation is only on a local scale. This effect will diminish if the cooled zone becomes larger towards the extent that the whole reservoir becomes cooled.

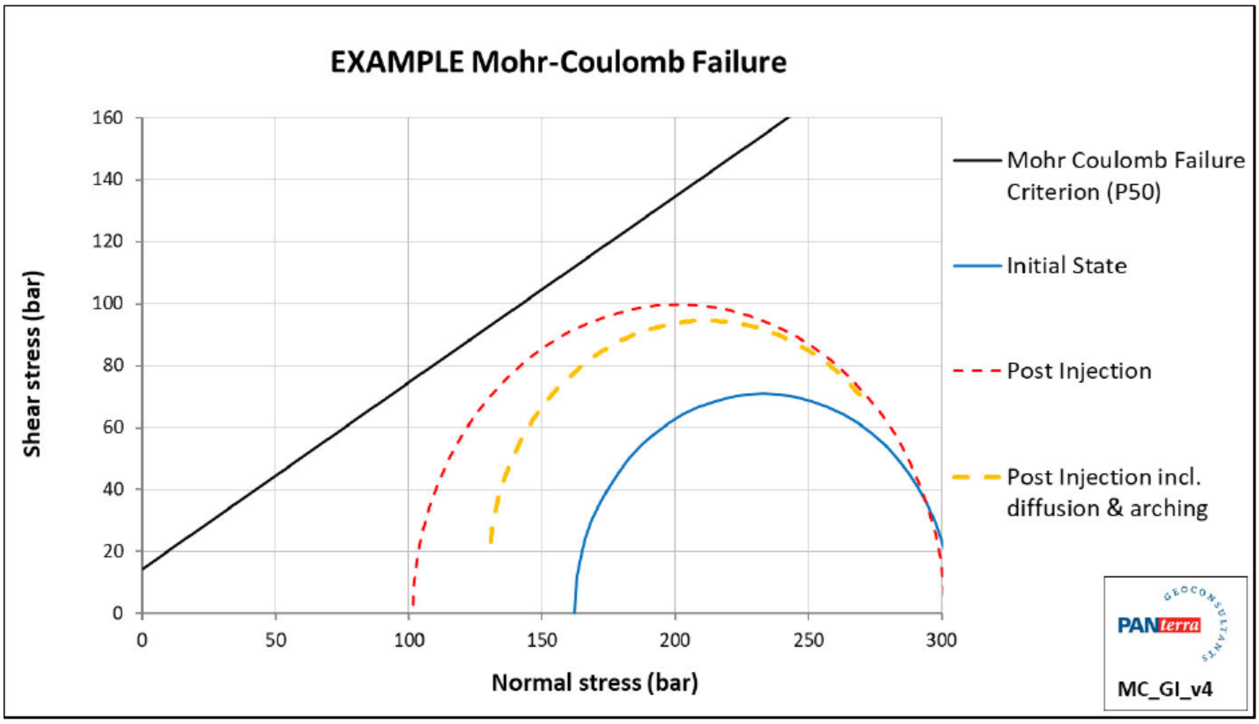

Figure 3-3 Mohr Coulomb model including temperature diffusion & arching. In the case of geothermal projects, the local higher stress concentrations along a fault can be offset by the fact that the stress perturbation is only on a local scale.

In a Mohr-Coulomb Monte-Carlo study, 1000 simulations are run on a large range of parameters covering the state of stress, production parameters, geological and rock parameters, fault parameters and arching and temperature diffusion. A triangular distribution is used to omit outliers as is consistent with the DoubletCalc approach, TNO (2014).

An example scenario is provided in Figure 3-4. The two Mohr-Circles are for reference and represent the median input (solid blue) and output (orange dashed) cases. The dots represent the output of the simulations where the red dots have an SCU above the P90-value and green dots have an SCU below the P10-value. Blue dots have SCU-values between P10 and P90-values. Any simulation exceeding the critical SCU > 1, and therefore exceeding the failure criterion, is indicated by a red square. The resulting P90, P50 and P10 failure criterion are displayed in the dashed linear lines. As the fault properties are varied for each individual simulation it may be possible that simulations exceed the P90 or even the P50 failure criterion without reaching the critical SCU > 1 as this is calculated separately for each individual scenario.

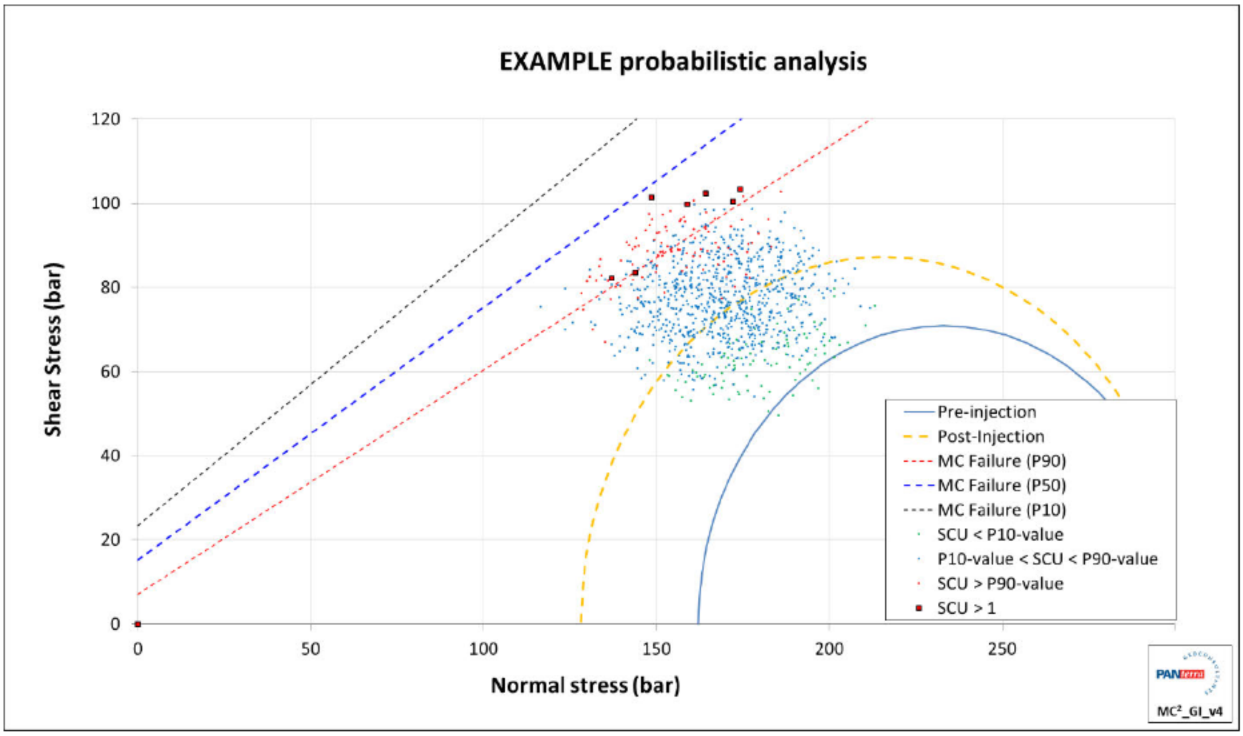

Figure 3-4 Mohr Coulomb Monte Carlo (*MC²*) model. The two Mohr-Circles are for reference and represent the median input (solid blue) and output (orange dashed) cases.

3.3 Temperature profile

The temperature profile is computed by our in-house fine-grid radial numerical reservoir simulation. An example is shown in Figure 3-5, which shows that our model predicts a more conservative (= larger) cold front radius than DoubletCalc2D. For reference, also the radius based on an analytical heat balance calculation is included. In the absence of thermal diffusion from cap- and baserock, the numerically computed centre of the cold front should coincide with this line.

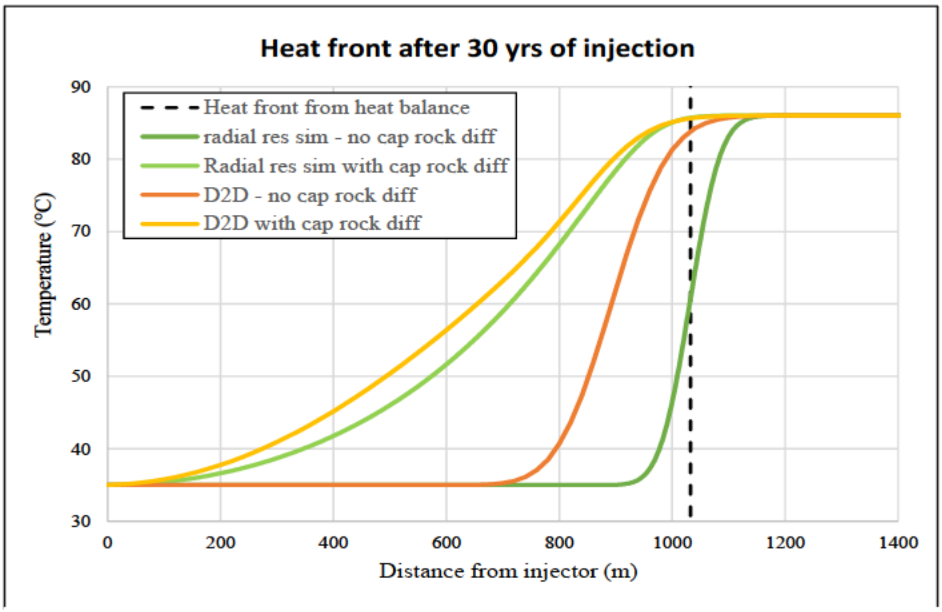

Figure 3-5 Temperature profiles as computed by our model and by DoubletCalc2D, both without and with thermal diffusion from cap- and baserock. Dashed line represents the position of the heat front based on analytical heat balance calculation. In the absence of thermal diffusion from cap- and baserock, the centre of the cold front should coincide with this line.

4 Geological and geomechanical setting

4.1 Geological setting

A geological study of the subsurface of Polanen was performed in 2018 (PanTerra, 2018), based on which a SDE+ subsidy application was performed and approved. In 2020, a seismic reinterpretation was performed (PanTerra, 2020a), which is the basis of current depth and thickness model. Reservoir properties are still based on the geological study of 2018.

The Polanen doublet will be situated in the West Netherlands Basin (Figure 4-1), which is an inverted rift basin (de Jager et al., 1996). Sediments in this basin range in age from Jurassic to recent and are overlying Triassic and older sediments. The reservoir targets is the Cretaceous Delft Sandstone Member. The Delft Sandstone has good reservoir properties in general.

In the Late Cretaceous, during the deposition of the Chalk Group, the West Netherlands Basin was inverted. This was accompanied by compressional movements and resulted in convergent oblique-slip faulting, general uplift, erosion and basin inversion, which reactivated pre-existing normal faults. The major tectonic feature in the region of the license is a NW-SE trending half graben. The structure is bounded by two faults (i.e., F1 and F4 as indicated in Figure 4-2).

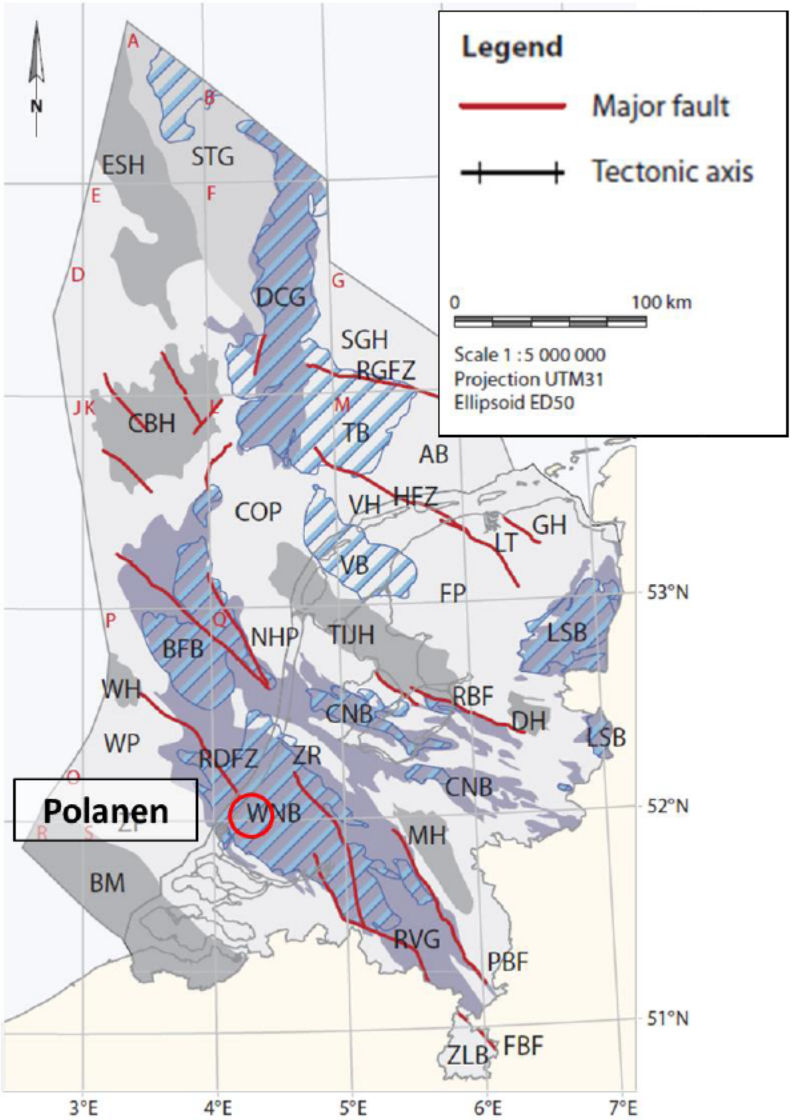

Figure 4-1 Structural elements and major fault zones as present during the Late Jurassic-Early Cretaceous (Duin et al., 2006).

At reservoir level, injector MON-GT-02 is located approximately 625-725 m away from faults (Figure 4-2 and Table 4-1). Producer MON-GT- 01 is planned approximately 200-500 m away from the nearest fault, a N-S oriented fault west of MON-GT-01. There is some uncertainty on the exact location of this fault. Figure 4-2 and Figure 4-3 show seismic cross sections perpendicular to the azimuth of the faults. Note that fault F3 is disappearing in the direction of injector MON-GT-02, as its fault throw is diminishing. No faults are observed between the two wells. The two major faults bounding the structure are regarded as sealing because of their large throw. Possible subseismic faults are unlikely to be sealing since the reservoir thickness is greater than the seismic resolution.

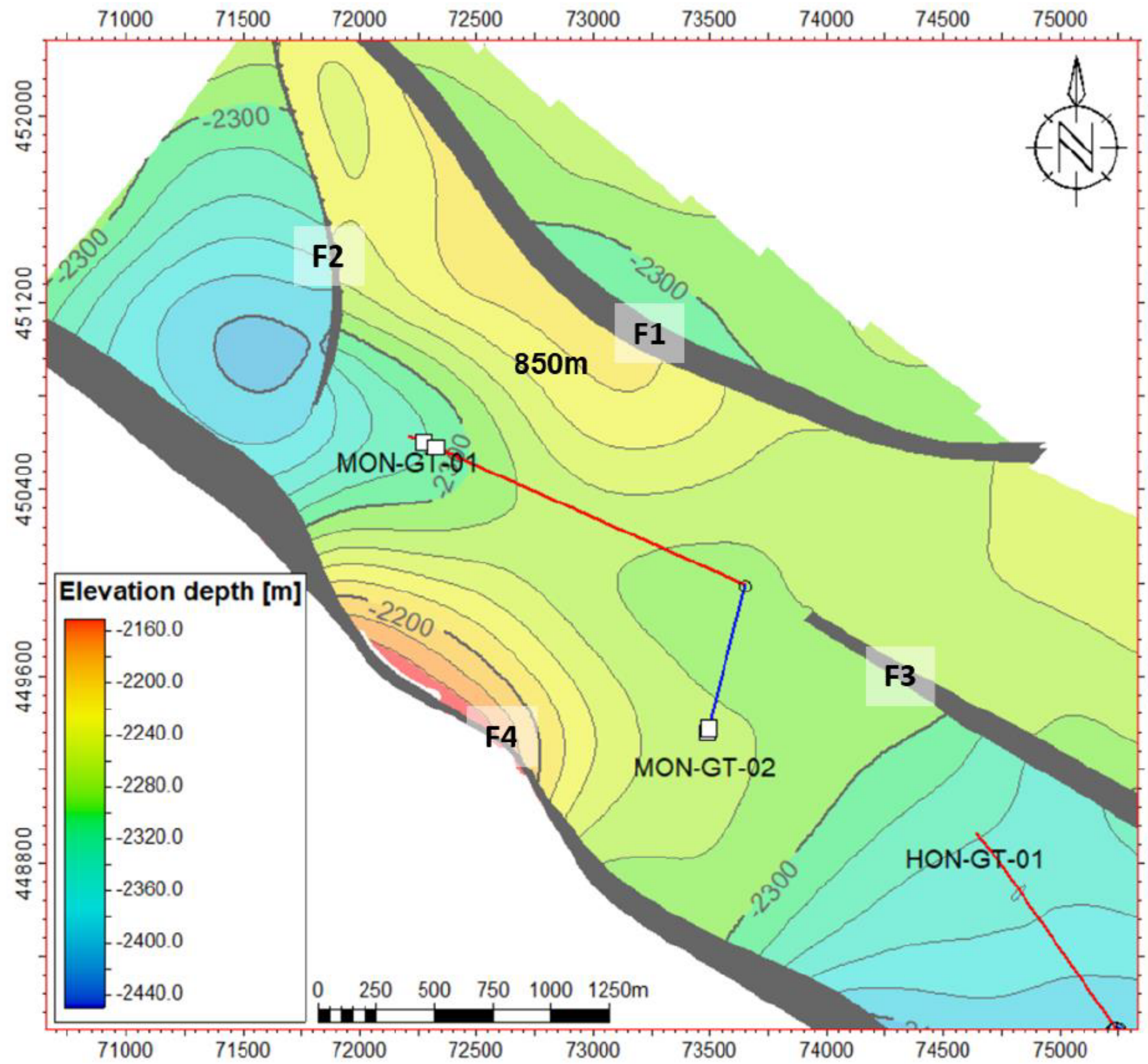

Figure 4-2 Top Delft reservoir depth map of the target area with planned wells, penetration points (white squares) and faultlines (grey, F1 to F4).

Table 4-1 Faults and geometrical information for injection well MON-GT-02.

Fault	Offset (m)	Distance to injector @ top reservoir (m)
F3	0-20	~625
F4	~75	~725

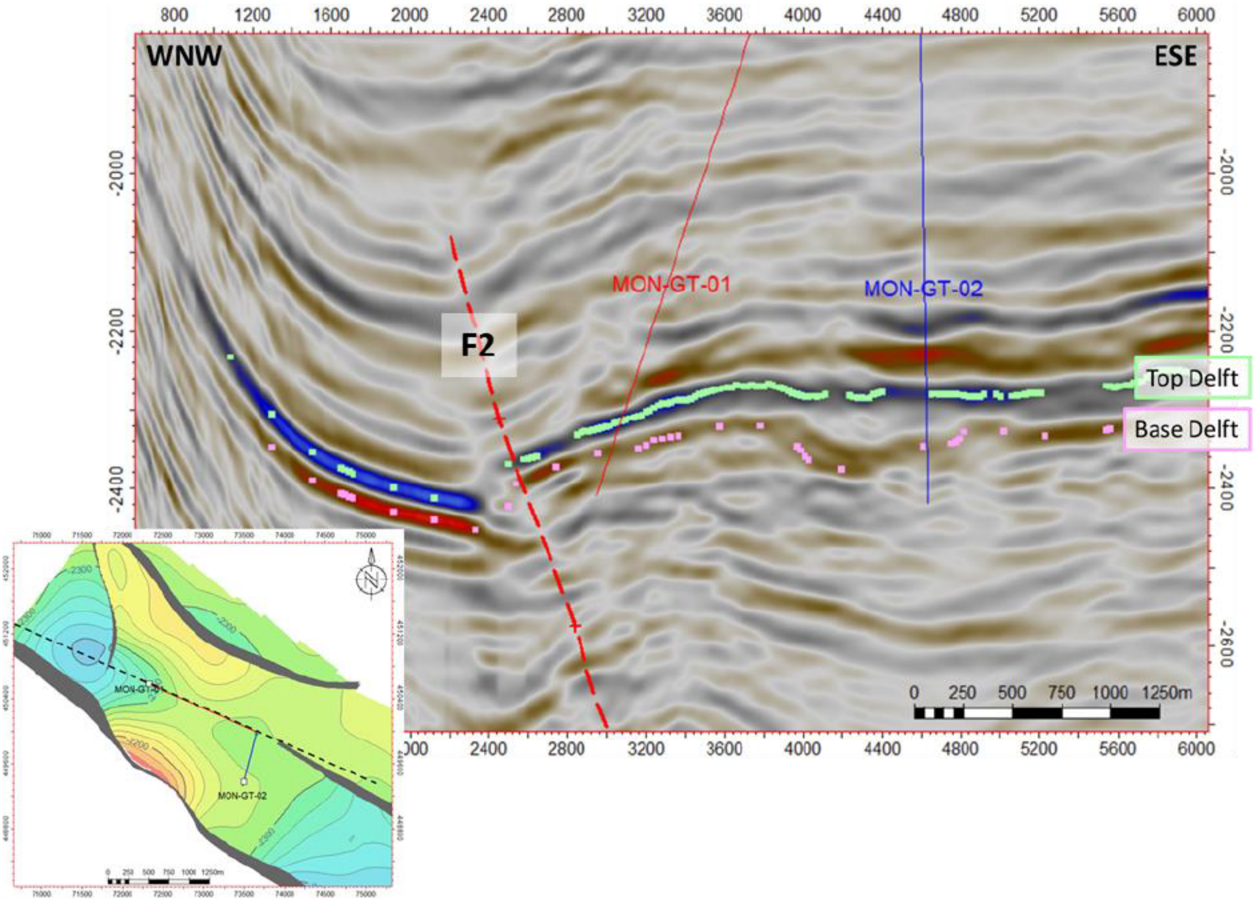

Figure 4-3 Seismic cross-section with projections of well MON-GT-01 and -02. Profile location and fault codes (F1 to F4) in Figure 4-2.

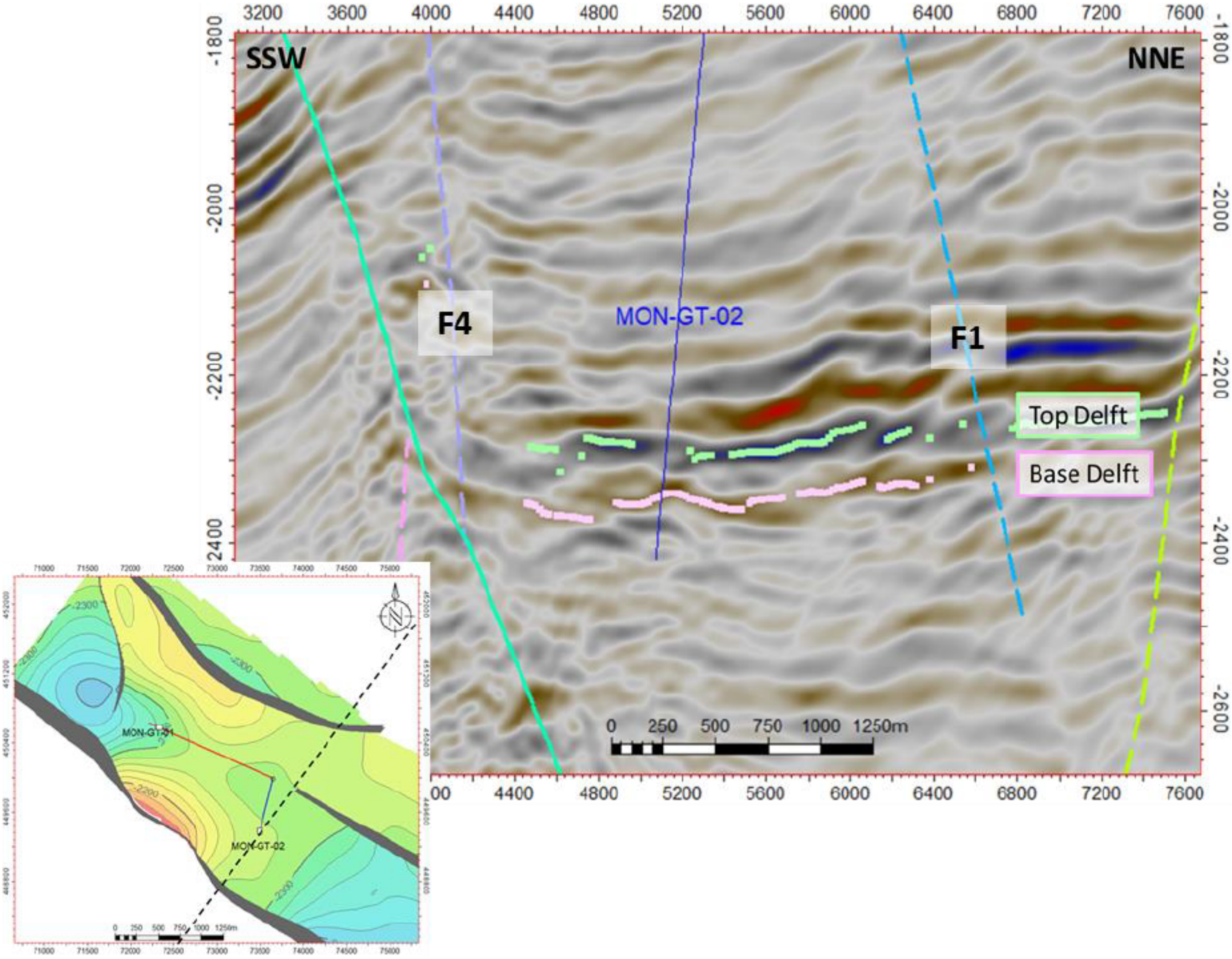

Figure 4-4 Seismic cross-section with projections of well MON-GT-02. Profile location and fault codes (F1 to F4) in Figure 4-2.

4.2 In-situ stress estimates

In-situ stress trends are mostly based on measured leak-off pressures as reported by Verweij et al. (2012). These authors distinguished a number of different geological areas within the Netherlands. For each of these areas, an in-situ stress trend map was generated. The geological area that is relevant for the current discussion is the so-called West Netherlands Basin for which the data are given in Figure 4-5. This figure displays measured Formation Integrity Tests (FIT) / leak-off pressure tests (LOT) as a function of depth in the West Netherlands platform area.

Until a depth of around 1500 m, the trend closely follows the well-known minimum in-situ stress gradient of 0.158 bar/m (0.7 psi/ft) for an extensional stress regime, whilst at greater depths it starts to bend somewhat towards higher stresses.

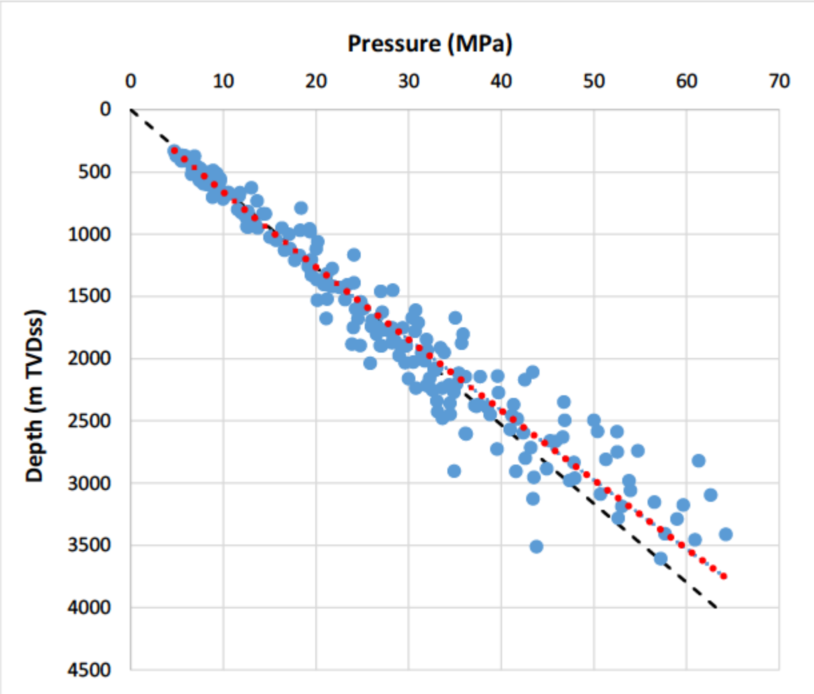

Figure 4-5 Minimum in-situ stress versus depth trend in the West Netherlands Basin area based on Formation Integrity Tests (FIT) / Leak-Off Tests (Verweij et al., 2012). Red-dashed line: trend line based on leak-off tests. Black-dashed line: trend line of 0.158 bar/m.

From the dataset shown in Figure 4-5, a subset was chosen from wells in the neighborhood of Polanen. The wells chosen plus the resulting stress trend are displayed in Figure 4-6. As can be seen, the baseline trend falls more or less on top of the well-known trend of 0.158 bar/m for an extensional stress regime, with a standard deviation of 0.02 bar/m.

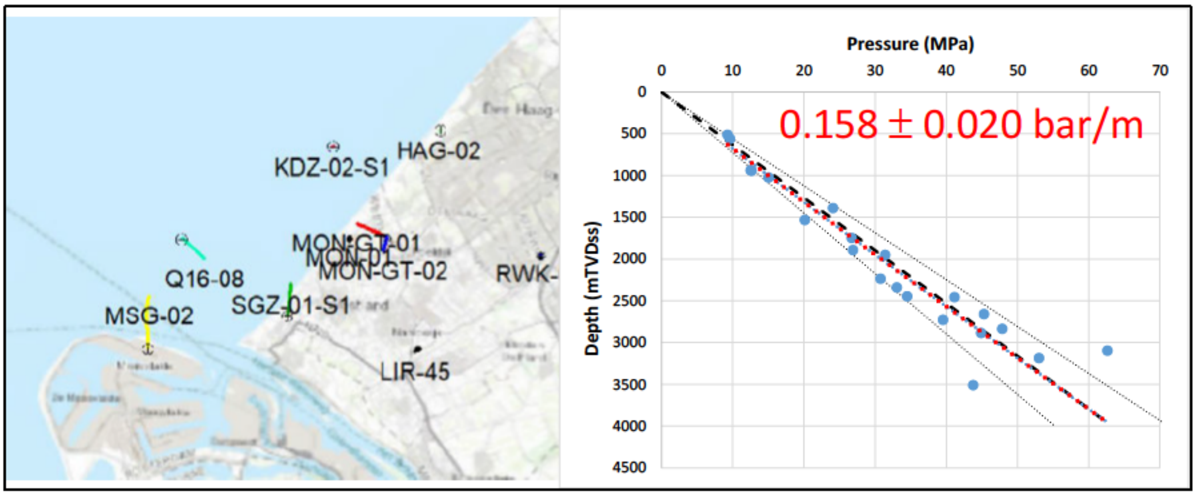

Figure 4-6 Minimum in-situ stress versus depth trend in the West Netherlands Basin area based on Formation Integrity Tests (FIT) / Leak-Off Tests from wells in the neighborhood of Polanen.

4.3 Reservoir Parameters

Reservoir parameters have influence on both the production prognosis as the geomechanical calculation and will be shortly discussed below.

4.3.1 Porosity and permeability

Porosity based on petrophysics of is expected to be 17 % in the Delft. The permeability used is 550 mD for the Delft.

4.3.2 Depth

Top of the reservoir is reported at 2276 m TVD for the Delft.

4.3.3 Thickness

The median thickness of the Delft is estimated to be 47 m.

4.3.4 Temperature

Based on data from Doubletcalc, reservoirs temperature has been set to 86°C.

4.3.5 Thermo-elastic constant

In response to temperature changes, the reservoir rock will tend to expand (heating) or shrink (cooling). Because in the subsurface there is no 'room' in the horizontal direction to expand or shrink ('plane strain'), this results in a change of total horizontal stress that is given by

$$\Delta\sigma_{\mathrm{h}} = A_{\mathrm{T}}.\Delta T \qquad (1)$$

where ΔT is the temperature change (negative for cooling) and A_T is the "thermo-elastic constant" (in bar/°C). Equation (1) is only valid if the entire reservoir has been cooled. When only part of the reservoir has been cooled, a geometry correction factor is applied. This geometry correction factor is also included in the fracture simulator.

The thermo-elastic constant is a material property of the rock. Under the assumption of perfectly elastic behaviour of the rock, both at matrix level and at grain level, this constant can be expressed as

$$A_{\mathrm{T}} = \frac{\alpha E}{1-\nu} \qquad (2)$$

where

- α is the linear thermal expansion coefficient (in $°C^{-1}$)
- E is Young's modulus (in bar)
- ν is poisson's ratio (dimensionless)

suggesting that A_T is linearly proportional to Young's modulus E if the thermal expansion coefficient α is assumed equal for all types of rocks under all circumstances (stress, temperature, ..).

Not many measurements of this constant have been carried out. Koning (1988) and Perkins & Gonzalez (1985) used values for A_T in the range 0.9-1.0 bar/°C for 'medium-strength' reservoir sandstones with Young's moduli in the range 10-15 GPa. For deep, tight rocks (> 10000 ft TVD), values of A_T in the range 1.5-2.0 bar/°C have been used in a number of oil field studies with waterflooding, both in Prudhoe Bay, Alaska (Stevens et al., 2000) and in the North Sea (Santarelli et al., 2008; Svendsen et al., 1991). On the other hand, in the Eider oil field, North Sea (~ 9000 ft TVss) a value of A_T = 0.6 bar/°C was derived based on step-rate tests, whilst in a carbonate / mudstone reservoir in the Middle East (~6500 ft tVD), a range of 0.4-0.9 bar/°C was measured on different core plugs. From the above we derive an average value for

A_T of ~1.0 ± 0.5 bar/°C, which may increase up to ~ 2,0 bar/°C for (very) tight rocks. In the current study a value of 1.0 ± 0.5 bar/°C is used

4.3.6 Poro-elastic constant

In response to pressure changes, the reservoir rock will tend to expand (pressurisation) or shrink (depletion). Because in the subsurface there is no 'room' in the horizontal direction to expand or shrink ('plane strain'), this results in a change of total horizontal stress that is given by

$$\Delta\sigma_{\mathrm{h}} = A_{\mathrm{p}}.\Delta p \tag{3}$$

where Δp is the pressure change (negative for depletion) and A_p is the "poro-elastic constant" (dimensionless). Equation (3) is only valid if the entire reservoir has been pressurised or depleted. When only part of the reservoir has been pressurised / depleted, a geometry correction factor is applied. This geometry correction factor is also included in the fracture simulator.

The poro-elastic constant is a material property of the rock. Under the assumption of perfectly elastic behaviour of the rock, both at matrix level and at grain level, this constant can be expressed as

$$A_{\mathrm{p}} = (1-\beta)\frac{1-2\nu}{1-\nu} \tag{4}$$

where

- $\beta = \frac{K_m}{K_s}$
- K_{m} is the bulk modulus of the rock matrix (bar)
- K_s is the bulk modulus of the solid rock grains (bar)

In practice, the above equation is only of qualitative value. Laboratory tests have shown that A_p often deviates significantly from the formula (4). Typical values are in the range 0.5-0.8. In the current study a value of 0.6 is used. Contrary to the thermo-elastic constant A_T, the value used for A_p is less critical because in a typical geothermal doublet, only a very small area around the injector is pressurised and only a small area around the producer is "depleted". On the other hand, a significant area around the injector will be cooled during the field life, thus making the parameter A_T a more critical one.

4.3.7 Fault parameters

Fault stability is defined by the cohesion and friction coefficient of the fault.

4.3.7.1 Cohesion

As a conservative low base, zero cohesion is assumed. For the probabilistic analysis a range of 0-15-30 bar is considered. A cohesion of 15 bar can be considered as 'typical' for weakly consolidated rock.

4.3.7.2 Friction coefficient

No measurements on fault properties are available. A typical sandstone has a friction coefficient in the order of ~0.6 (Hunfeld et al., 2017). Uncertainty ranges on sandstone are reported between 0.48 and 0.72 (Samuelson & Spiers, 2012). A range of 0.48-0.60-0.72 is used. No hardening and/or softening of the fault is considered in this analysis.

5 Results

5.1 Injector well MON-GT-02 – injection into the Delft formation – F3 fault

Results of F3 fault stability will be presented for four different times: 0 years (before start of operation), 10, 20 and 30 years. Figure 5-1 shows the geometric lay-out of the F3-fault together with the position of the MON-GT-02 injector. Cold front positions after 30 years of injection (end of field life) are indicated as well. The case of 30 years injection will be discussed further down below.

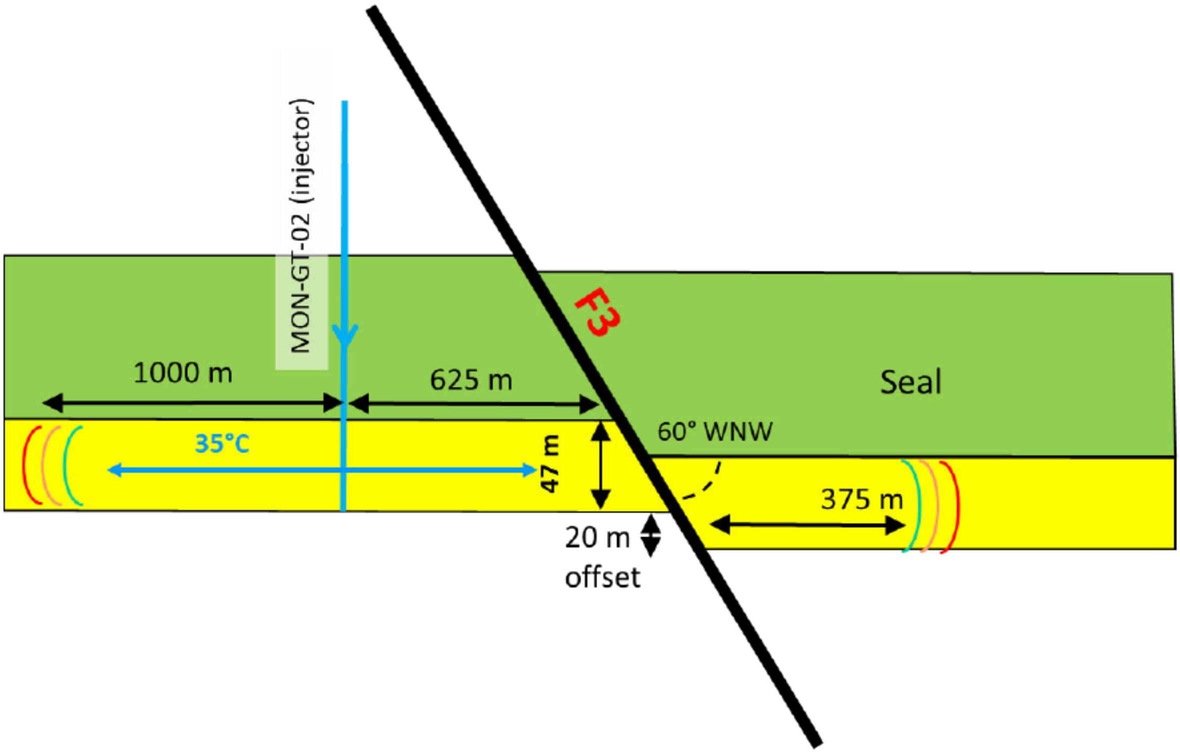

Figure 5-1 MON-GT-02 Delft F3: Side view (cross section) of injector, the fault and computed extent of the cooled zone at the end of field life.

5.1.1 0 years of injection (before start of injection).

5.1.1.1 Deterministic analysis

To start with, a fault stability analysis prior to injection was carried out with the objective to have a "reference case" of stability with which the impact of different injection periods can be compared. As is well-known, the "reference case"-situation can have an important impact on the feasibility of a geothermal project. For example, if in the reference case, the shear stress on the fault is already close to its maximum allowable value for fault reactivation, cold water injection will be not or hardly feasible. An well-known example of such a situation in The Netherlands is Limburg.

Figure 5-2 shows the situation and corresponding SCU for the Polanen case. As can be seen, the pre-injection SCU of the fault is equal to approximately 0.55 for the base case parameter values.

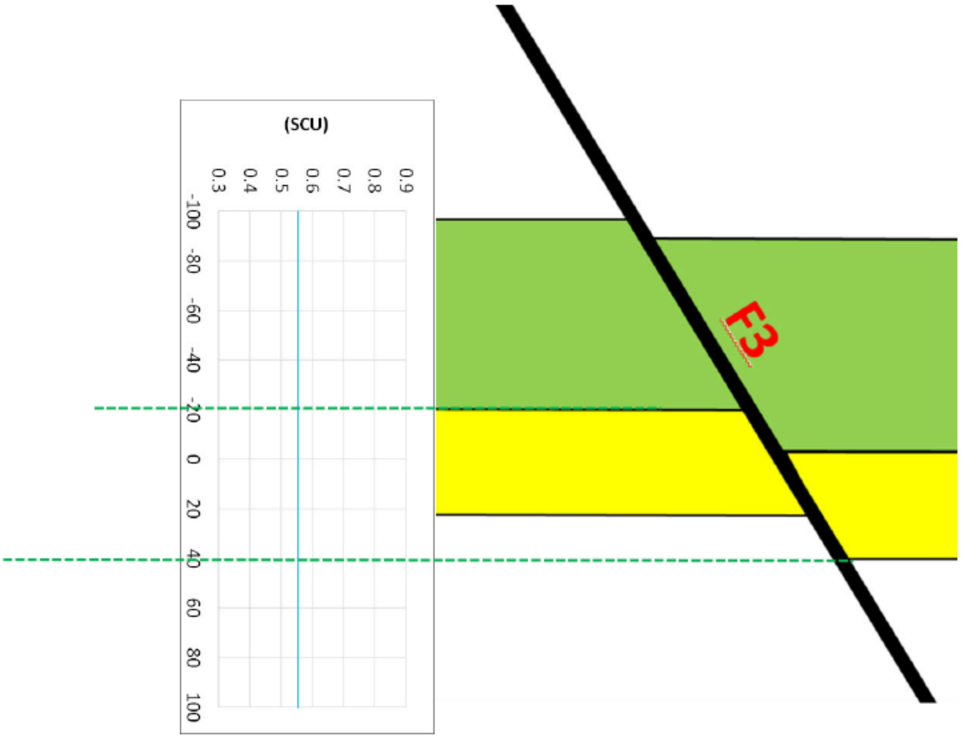

Figure 5-2 MON-GT-02 0 years, Delft F3: Computed SCU along the fault at the before start of injection.

5.1.1.2 Probabilistic analysis (Monte Carlo)

In order to address the impact of parameter uncertainties, a Mohr-Coulomb Monte-Carlo analysis was carried out using an ensemble of 1000 members. The addressed uncertain parameters are shown in Table 5-1, which displays the input parameters for the probabilistic analysis of the Delft formation and the F3 fault, including their low-med-high values. The parameters and reasoning have been discussed in section 4.3. Because for zero injection, the injector distance to the fault is irrelevant, and therefore this uncertainty has not been included in the current analysis (indicated by strikethrough in the table).

Table 5-1 Input parameters for probabilistic analysis of the Delft formation and the F3 Fault. See text for discussion.

	Parameter	Min	Median	Max
Rock Parameters	Reservoir Temperature (°C)	83	86	89
	Thermoelastic coefficient (bar/°C)	0.5	1.0	1.5
	Vertical stress gradient (bar/m)	0.21	0.22	0.23
	Horizontal stress gradient (bar/m)	0.144	0.158	0.189
Fault Parameters	Cohesion (bar)	0	15	30
	Friction coefficient (-)	0.48	0.60	0.72
	Dip (degrees)	50	60	70
	~~Distance from injector (m)~~	~~525~~	~~625~~	~~725~~

The results of this analysis are shown in Figure 5-3 and Figure 5-4. The majority of SCU values seen are in the 0.4-0.7 range, with 0.8% having an SCU between 0.9 and 1 (based on the P90 Mohr-Coulomb failure line), and 0.2% an SCU > 1 (based on the P90 Mohr-Coulomb failure line).

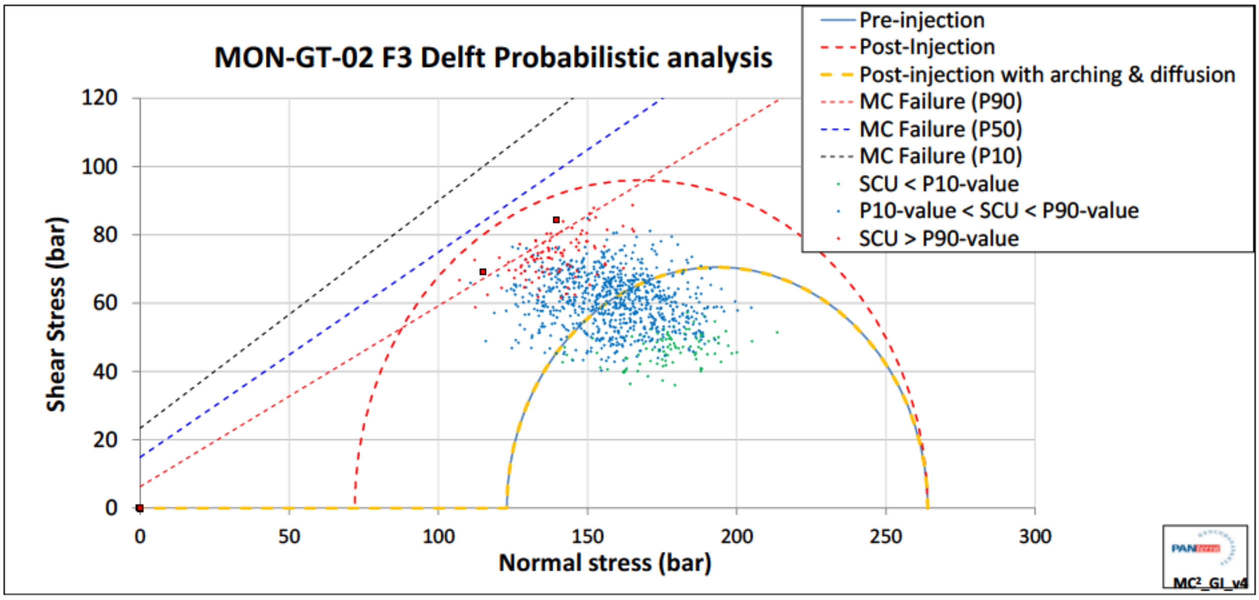

Figure 5-3 Results of Mohr-Coulomb Monte-Carlo for the F3 fault prior to injection into MON-GT-02. The dots represent the simulations, colours indicating the P10,P50 and P90 results. Three reference Mohr Circles are presented based on the median input: initial state (blue solid circle), result assuming full reservoir cooling (red-dashed circle) and result including arching & temperature diffusion (orange-dashed circle). Please note that in this case, the blue and orange-dashed circles coincide because no cold water has been injected (yet).

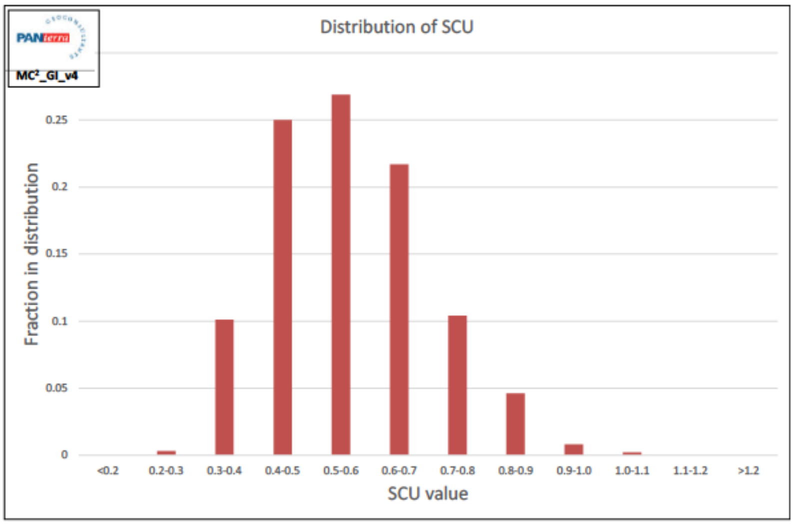

Figure 5-4 Probability diagram of the simulated SCU values prior to injection. The bulk of the values are in the <0.9 range, with 0.8% between 0.9 and 1 (based on the P90 Mohr-Coulomb failure line), and 0.2% with SCU > 1.0 (based on the P90 Mohr-Coulomb failure line).

5.1.2 10 years of injection

5.1.2.1 Temperature profile

The computed temperature profile away from the injector after 10 years of injection is presented in Figure 5-5. The cooled zone is not an abrupt front but rather influenced by thermal diffusion, both within the reservoir and from the cap- and baserock into the reservoir.

After 10 years of injection we observe a temperature alteration up to 600 m. This is considered the cold water "front". The F3 fault is expected at 625 m. This scenario is schematically depicted in Figure 5-5.

Based on the seismic, the fault offset is uncertain: between 0 and 20 m (Table 4-1). Within this range, the most conservative fault offset was chosen. This is equal to 20 m in this case.

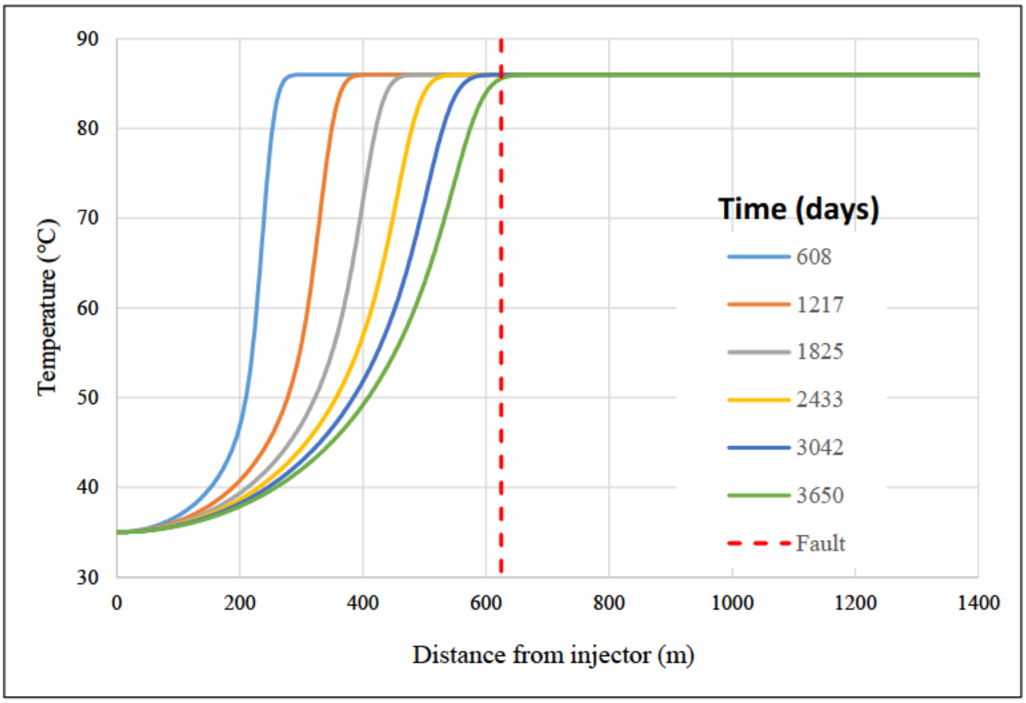

Figure 5-5 Temperature profile in the reservoir away from the injector after 10 years of injection.

5.1.2.2 Deterministic analysis

The methodology as described in Section 3.1 is applied to estimate the impact of the cooling on the Shear Capacity Utilisation (SCU). In order to take into account the effect of partial cooling, the entire temperature profile in the cooled zones to the left and to the right of the fault is computed. Subsequently, the thermo-elastic stress change on the fault resulting from this temperature profile is calculated. As a fault position is a matter of interpretation and faults often display 'damage zones' an uncertainty was taken into account in the fault position of ±100m.

The results are given in Figure 5-6 where the SCU is calculated for the initial state as well as the state of fault affected by a nearby cooled area. This shows the computed SCU along the fault after 10 years of injection. As can be seen, the maximum SCU (e.g. at vertical coordinate $x \approx 50$ m) is around 0.69 which is still significantly below 1. Varying the fault distance over ±100 m with respect to base case of 625 m from injector results in an SCU-variation between 0.58 and 0.69.

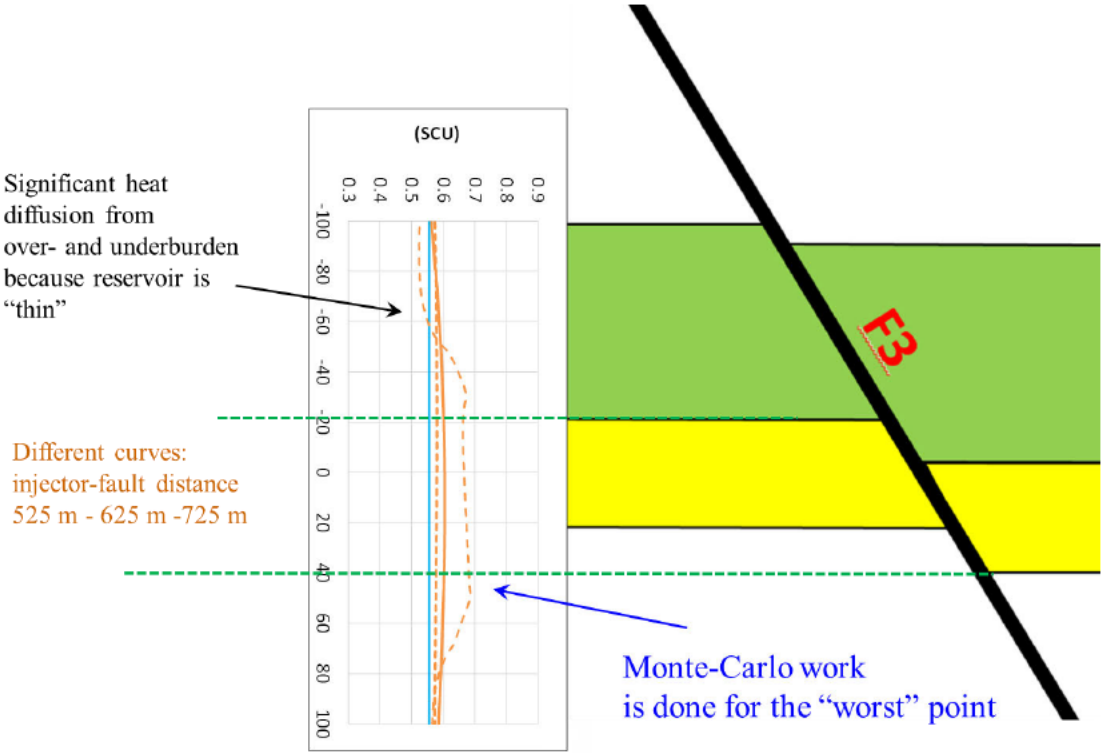

Figure 5-6 Computed SCU along the fault after 10 years of injection. The "worst point" is addressed in a Monte-Carlo simulation. Dashed lines indicate the results based on a fault uncertainty of ±100m.

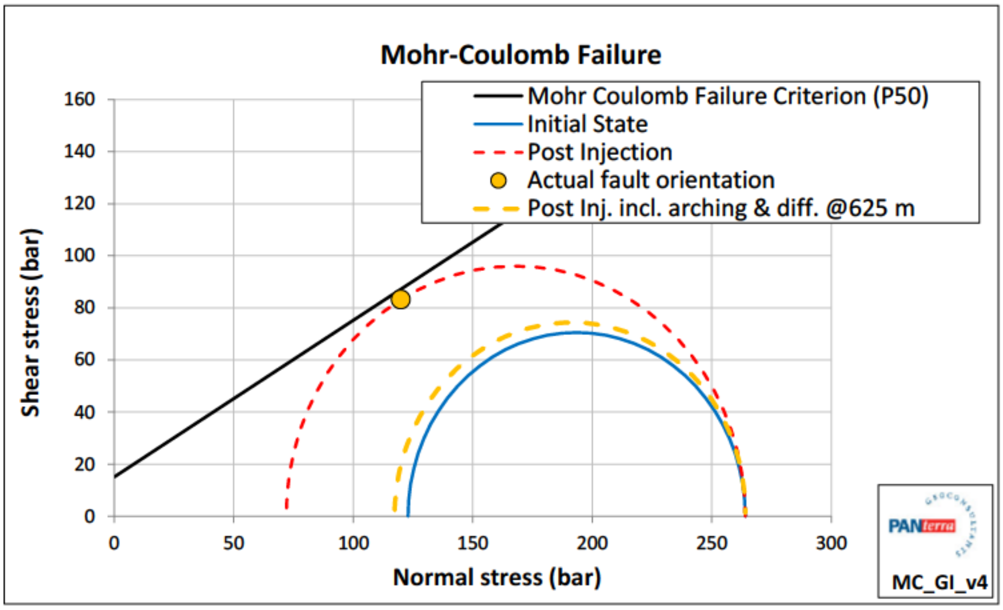

Figure 5-7 Mohr circles after 10 years of injection for the Delft formation at the "worst" point along the fault (see fig. 5-6).

Figure 5-7 shows a deterministic failure analysis for the "worst" point on the SCU curve of Figure 5-6. This figure shows the Mohr circles at the beginning of field life and after 10 years of injection for the base case scenario of a transmissible fault at 625 m. The red dashed Mohr circle is obtained by assuming a uniform cooling down to the injection temperature of 35°C across the entire reservoir. The yellow dashed Mohr circle includes the actual change of state of stress as a result of the cooled area, i.e. it includes the impact of stress arching by uncooled areas further away from the injector. Also, the approach presented here includes the impact of stress concentrations along the fault.

It should be noted that the impact of stress arching is very pronounced in this case (Figure 5-7). This can be explained by the fact that the lateral extent of the cooled zone around the fault is not (yet) very large compared to the reservoir thickness. As will be shown below, with progressing injection, the degree of stress arching decreases, in line with expectations.

5.1.2.3 Probabilistic analysis (Monte Carlo)

In order to address the impact of parameter uncertainties, a Mohr-Coulomb Monte-Carlo analysis was carried out using an ensemble of 1000 members. The addressed uncertain parameters are shown in Table 5-2, which displays the input parameters for the probabilistic analysis of the Delft formation and the F3 fault, including their low-med-high values. The parameters and reasoning have been discussed in section 4.3.

The results of this analysis are shown in Figure 5-8 and Figure 5-9. The Mohr circles shown are the same as those in Figure 5-7. The majority of SCU values seen are in the 0.4-0.8 range, with 4% having an SCU between 0.9 and 1 (based on the P90 Mohr-Coulomb failure line), and 1% an SCU > 1 (based on the P90 Mohr-Coulomb failure line).

In conclusion, after 10 years of injection, the likelihood of activation of the F3 fault by injecting 35°C water into the Delft formation via MON-GT-02 can be considered very small.

Table 5-2 input parameters for probabilistic analysis of the Delft formation and the F3 Fault.

	Parameter	Min	Median	Max
Rock Parameters	Reservoir Temperature (°C)	83	86	89
	Thermoelastic coefficient (bar/°C)	0.5	1.0	1.5
	Vertical stress gradient (bar/m)	0.21	0.22	0.23
	Horizontal stress gradient (bar/m)	0.144	0.158	0.189
Fault Parameters	Cohesion (bar)	0	15	30
	Friction coefficient (-)	0.48	0.60	0.72
	Dip (degrees)	50	60	70
	Distance from injector (m)	525	625	725

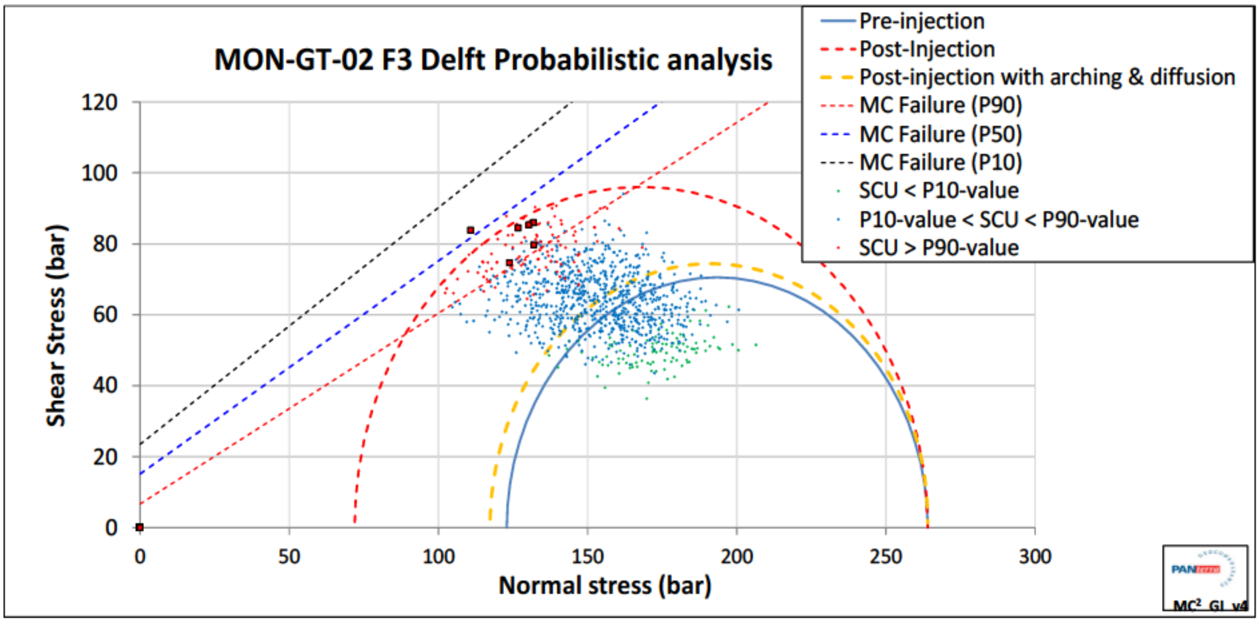

Figure 5-8 Results of Mohr-Coulomb Monte-Carlo for cooling around the F3 fault as a result of doublet MON-GT-02, after 10 years of injection The dots represent the simulations, colours indicating the P10,P50 and P90 results. Three reference Mohr Circles are presented based on the median input: initial state (blue solid circle), result assuming full reservoir cooling (red-dashed circle) and result including arching & temperature diffusion (orange-dashed circle).

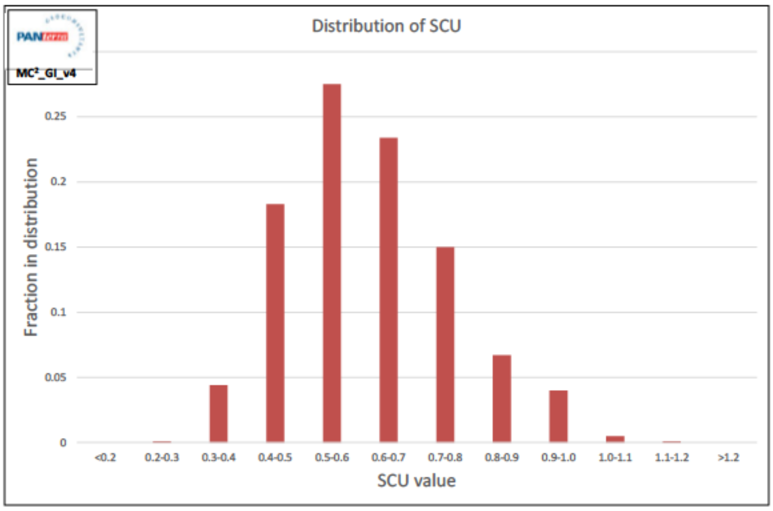

Figure 5-9 Probability diagram of the simulated SCU values after 10 years of injection. The bulk of the values are in between 0.4 and 0.8, with 4% between 0.9 and 1 (based on the P90 Mohr-Coulomb failure line), and 1% with SCU > 1.0 (based on the P90 Mohr-Coulomb failure line).

5.1.3 20 years of injection

5.1.3.1 Temperature profile

The computed temperature profile away from the injector after 20 years of injection is presented in Figure 5-10. The cooled zone is not an abrupt front but rather influenced by thermal diffusion, both within the reservoir and from the cap- and baserock into the reservoir. After 20 years of injection we observe a temperature alteration up to 850 m.

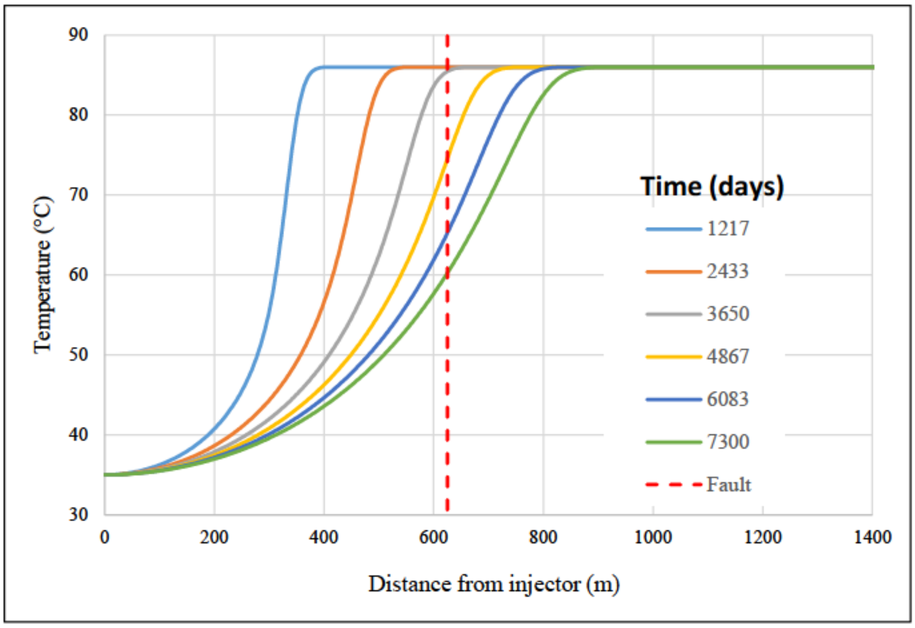

Figure 5-10 Temperature profile in the reservoir away from the injector after 20 years of injection.

5.1.3.2 Deterministic analysis

The results are given in Figure 5-11 where the SCU is calculated for the initial state as well as the state of fault affected by a nearby cooled area. This shows the computed SCU along the fault after 20 years of injection. As can be seen, the maximum SCU (e.g. at vertical coordinate x ≈ 40 m) is around 0.80 which is still significantly below 1. Varying the fault distance over ±100 m with respect to base case of 625 m from injector results in an SCU-variation between 0.66 and 0.80.

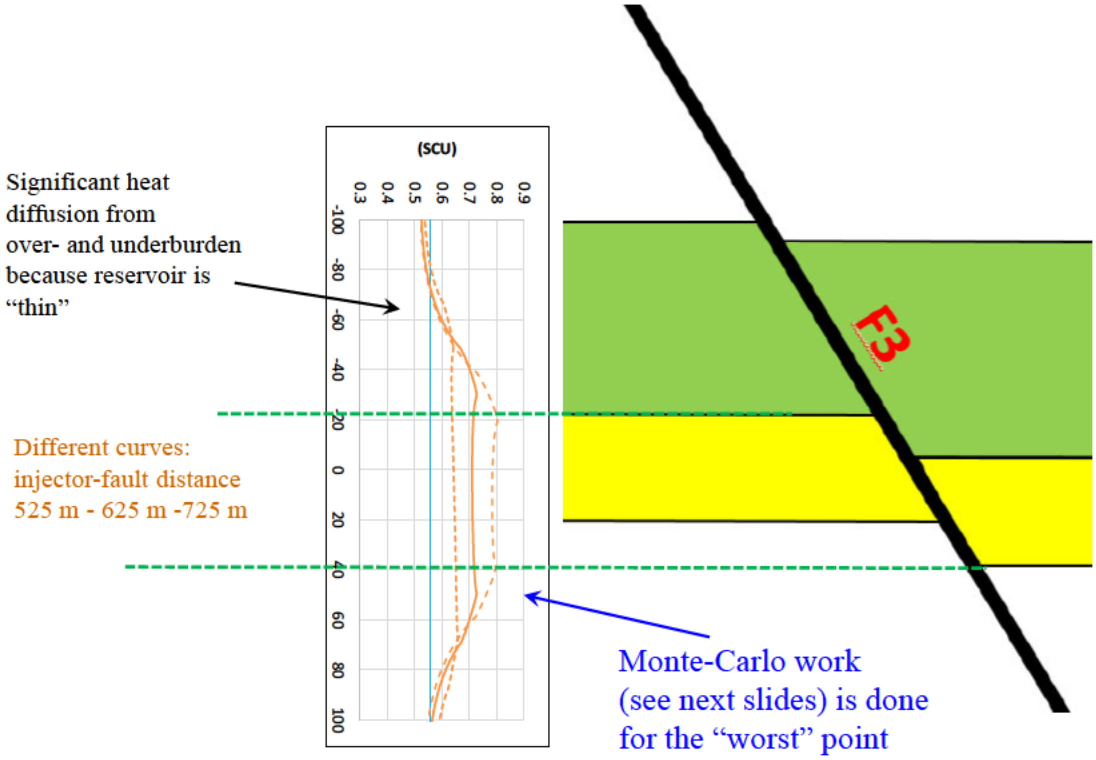

Figure 5-11 Computed SCU along the fault after 20 years of injection. The "worst point" is addressed in a Monte-Carlo simulation. Dashed lines indicate the results based on a fault uncertainty of ±100m.

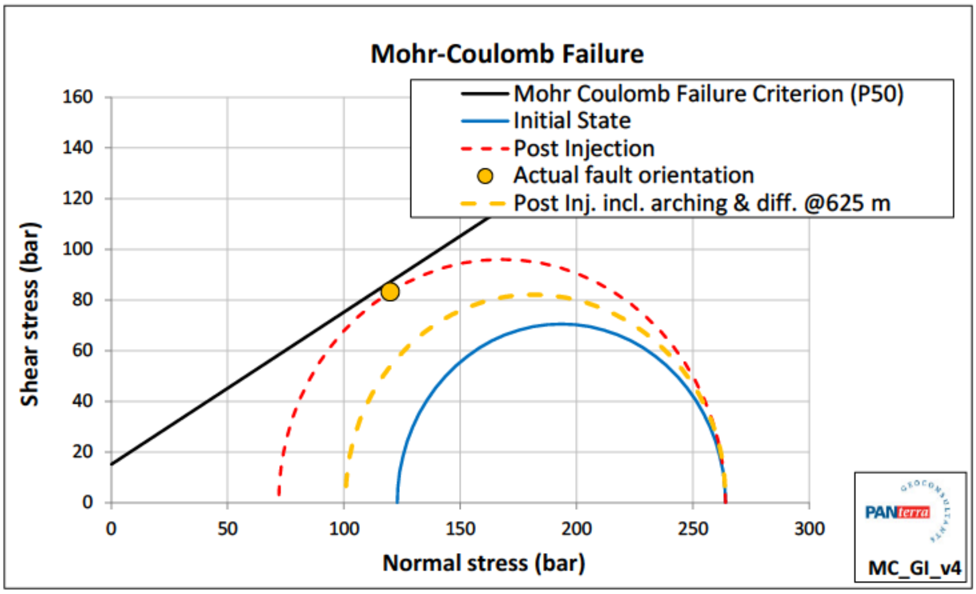

Figure 5-12 Mohr circles after 20 years of injection for the Delft formation at the "worst" point along the fault (see fig. 5-11).

Figure 5-12 shows a deterministic failure analysis for the "worst" point on the SCU curve of Figure 5-11. This figure shows the Mohr circles at the beginning of field life and after 20 years of injection for the base case scenario of a transmissible fault at 625 m. The red dashed Mohr circle is obtained by assuming a uniform cooling down to the injection temperature of 35°C across the entire reservoir. The yellow dashed Mohr circle includes the actual change of state of stress as a result of the cooled area, i.e. it includes the impact of stress arching by uncooled areas further away from the injector. Also, the approach presented here includes the impact of stress concentrations along the fault.

It should be noted that the impact of stress arching is still reasonably pronounced in this case (Figure 5-12), though less than after 10 years of injection (Figure 5-7). This can be explained by the fact that the lateral extent of the cooled zone around the fault is increasing but not (yet) very large compared to the reservoir thickness.

5.1.3.3 Probabilistic analysis (Monte Carlo)

In order to address the impact of parameter uncertainties, a Mohr-Coulomb Monte-Carlo analysis was carried out using an ensemble of 1000 members. The addressed uncertain parameters are shown in Table 5-2 above.

The results of this analysis are shown in Figure 5-13 and Figure 5-14. The Mohr circles shown are the same as those in Figure 5-12. The majority of SCU values seen are in the 0.5-0.9 range, with 8% having an SCU between 0.9 and 1 (based on the P90 Mohr-Coulomb failure line), and 8% an SCU > 1 (based on the P90 Mohr-Coulomb failure line).

In conclusion, after 20 years of injection, the likelihood of activation of the F3 fault by injecting 35°C water into the Delft formation via MON-GT-02 can no longer be considered very small.

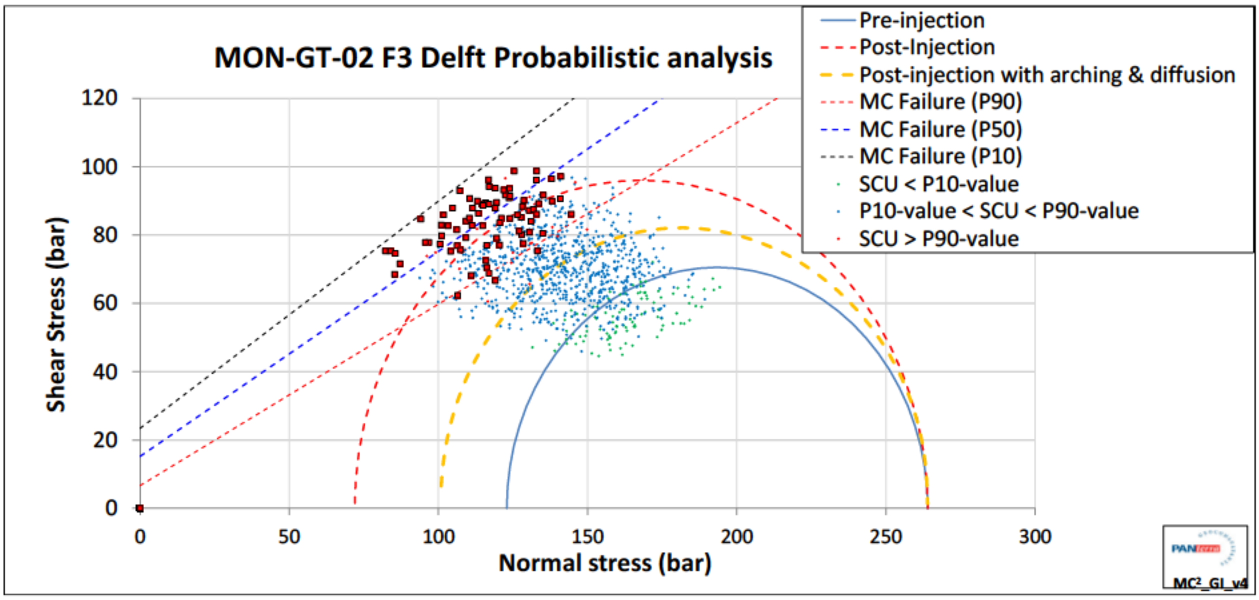

Figure 5-13 Results of Mohr-Coulomb Monte-Carlo for cooling around the F3 fault as a result of doublet MON-GT-02, after 20 years of injection The dots represent the simulations, colours indicating the P10,P50 and P90 results. Three reference Mohr Circles are presented based on the median input: initial state (blue solid circle), result assuming full reservoir cooling (red-dashed circle) and result including arching & temperature diffusion (orange-dashed circle).

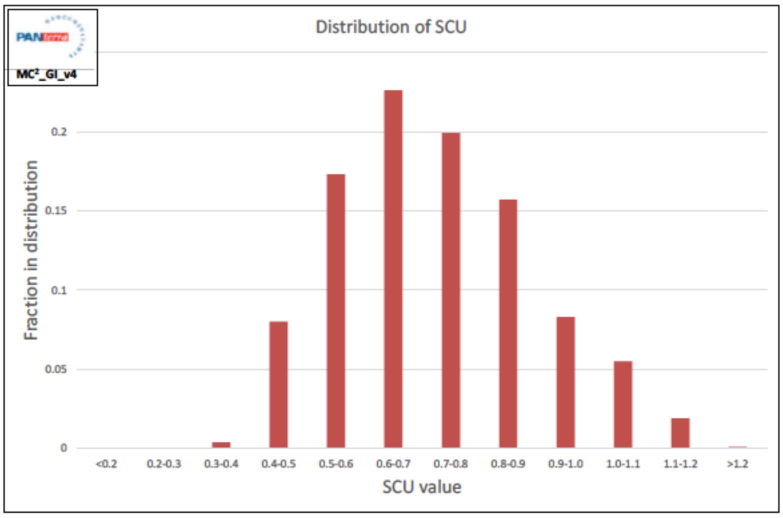

Figure 5-14 Probability diagram of the simulated SCU values after 20 years of injection. The bulk of the values are in between 0.5 and 0.9, with 8% between 0.9 and 1 (based on the P90 Mohr-Coulomb failure line), and 8% with SCU > 1.0 (based on the P90 Mohr-Coulomb failure line).

5.1.4 30 years of injection

5.1.4.1 Temperature profile

The computed temperature profile away from the injector after 30 years of injection is presented in Figure 5-15. The cooled zone is not an abrupt front but rather influenced by thermal diffusion, both within the reservoir and from the cap- and baserock into the reservoir. After 30 years of injection we observe a temperature alteration up to 1000m.

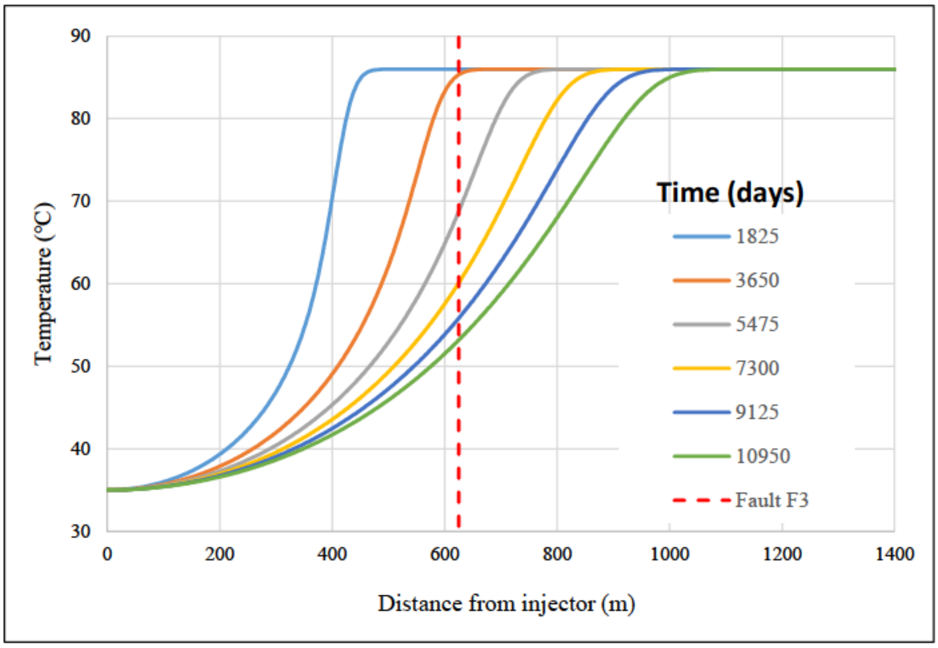

Figure 5-15 Temperature profile in the reservoir away from the injector after 30 years of injection.

5.1.4.2 Deterministic analysis

The results are given in Figure 5-16 where the SCU is calculated for the initial state as well as the state of fault affected by a nearby cooled area. This shows the computed SCU along the fault at the end of field life (30 years of injection). As can be seen, the maximum SCU (e.g. at vertical coordinate $x \approx 40$ m) is around 0.84 which is still well below 1. Varying the fault distance over ±100 m with respect to base case of 625 m from injector results in an SCU-variation between 0.72 and 0.80.

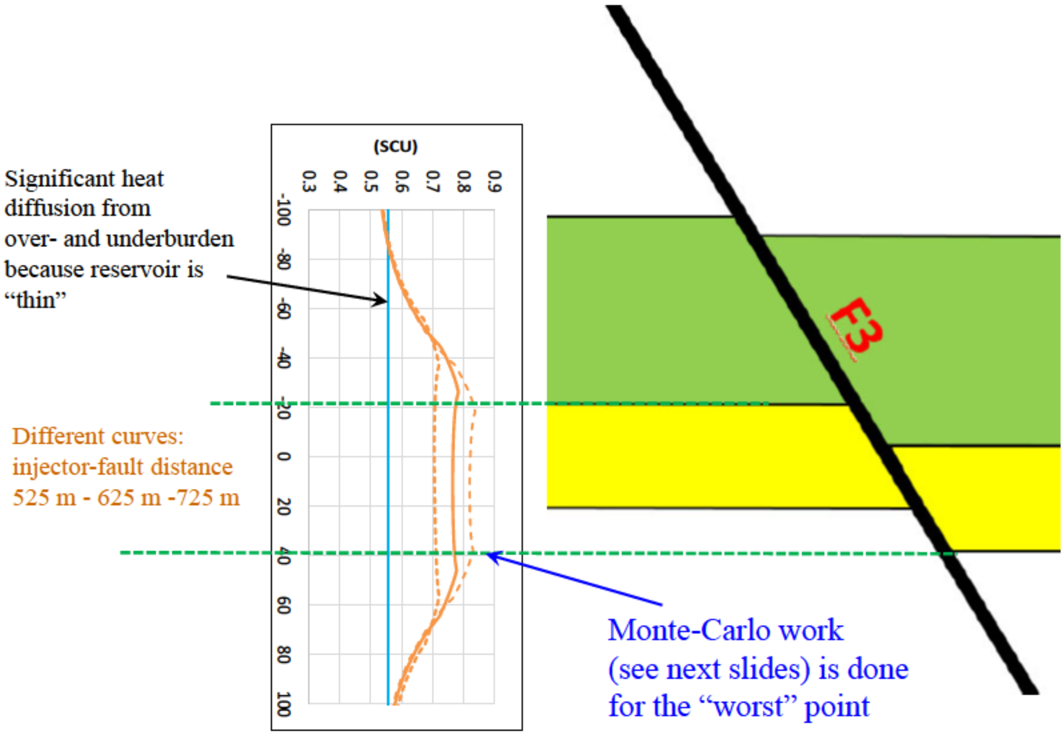

Figure 5-16 Computed SCU along the fault after 30 years of injection. The "worst point" is addressed in a Monte-Carlo simulation. Dashed lines indicate the results based on a fault uncertainty of ±100m.

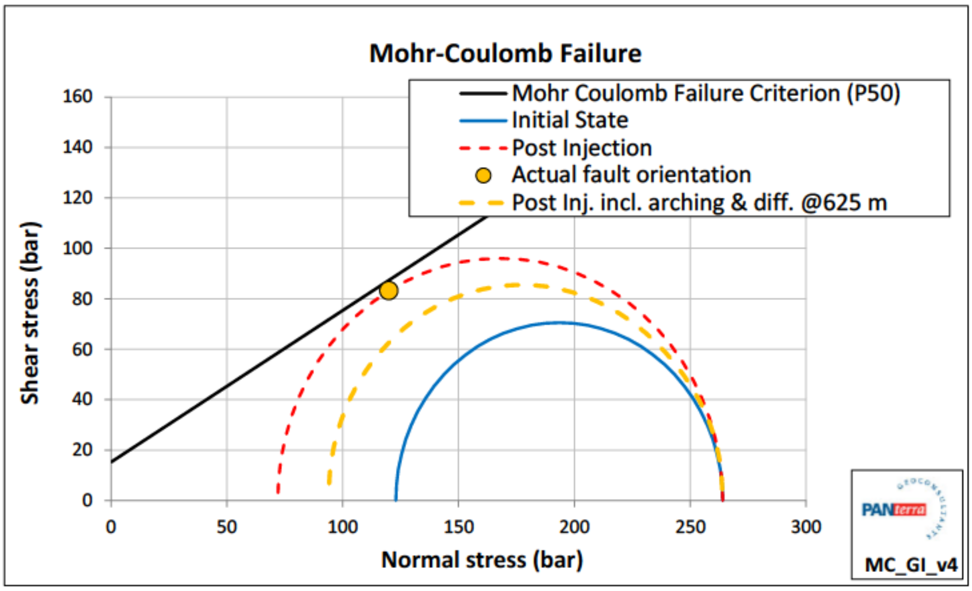

Figure 5-17 Mohr circles after 30 years of injection for the Delft formation at the "worst" point along the fault (see fig. 5-16).

Figure 5-17 shows a deterministic failure analysis for the "worst" point on the SCU curve of Figure 5-16. This figure shows the Mohr circles at the beginning of field life and after 30 years of injection for the base case scenario of a transmissible fault at 625 m. The red dashed Mohr circle is obtained by assuming a uniform cooling down to the injection temperature of 35°C across the entire reservoir. The yellow dashed Mohr circle includes the actual change of state of stress as a result of the cooled area, i.e. it includes the impact of stress arching by uncooled areas further away from the injector. Also, the approach presented here includes the impact of stress concentrations along the fault.

It should be noted that the impact of stress arching is still present in this case (Figure 5-17), though clearly less than after 10 and 20 years of injection (Figure 5-7 and Figure 5-12). This can be explained by the fact that the lateral extent of the cooled zone around the fault is starting to grow large compared to the reservoir thickness.

5.1.4.3 Probabilistic analysis (Monte Carlo)

In order to address the impact of parameter uncertainties, a Mohr-Coulomb Monte-Carlo analysis was carried out using an ensemble of 1000 members. The addressed uncertain parameters are shown in Table 5-2 above.

The results of this analysis are shown in Figure 5-18 and Figure 5-19. The Mohr circles shown are the same as those in Figure 5-17. The majority of SCU values seen are in the 0.5-1.0 range, with 12% having an SCU between 0.9 and 1 (based on the P90 Mohr-Coulomb failure line), and 11% an SCU > 1 (based on the P90 Mohr-Coulomb failure line).

In conclusion, after 30 years of injection, the likelihood of activation of the F3 fault by injecting 35°C water into the Delft formation via MON-GT-02 can be considered non-negligible.

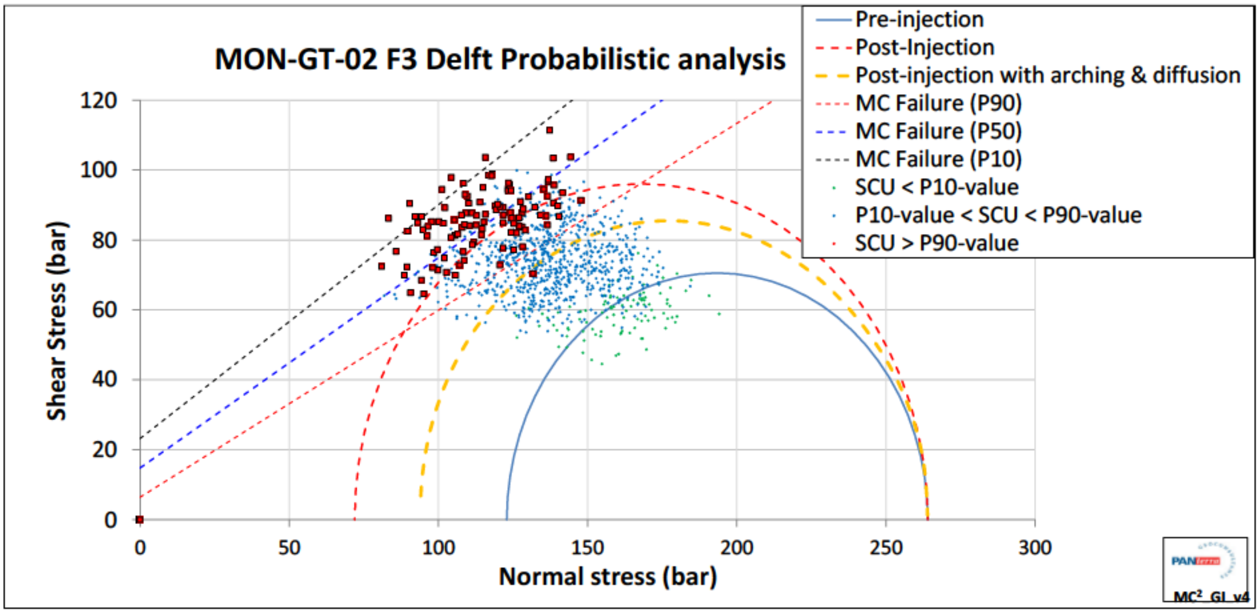

Figure 5-18 Results of Mohr-Coulomb Monte-Carlo for cooling around the F3 fault as a result of doublet MON-GT-02, after 30 years of injection The dots represent the simulations, colours indicating the P10,P50 and P90 results. Three reference Mohr Circles are presented based on the median input: initial state (blue solid circle), result assuming full reservoir cooling (red-dashed circle) and result including arching & temperature diffusion (orange-dashed circle).

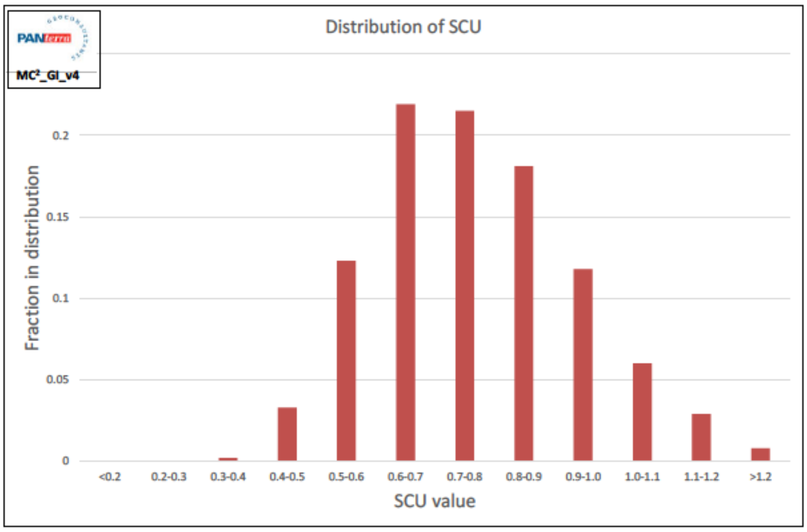

Figure 5-19 Probability diagram of the simulated SCU values after 30 years of injection. The bulk of the values are in between 0.5 and 0.9, with 8% between 0.9 and 1 (based on the P90 Mohr-Coulomb failure line), and 8% with SCU > 1.0 (based on the P90 Mohr-Coulomb failure line).

5.2 Injector well MON-GT-02 – injection into the Delft formation – F4 fault

Results of F4 fault stability will be presented for four different times: 0 years (before start of operation), 10, 20 and 30 years. Figure 5-20 shows the geometric lay-out of the F4-fault together with the position of the MON-GT-02 injector. Cold front positions after 30 years of injection (end of field life) are indicated as well. The case of 30 years injection will be discussed further down below.

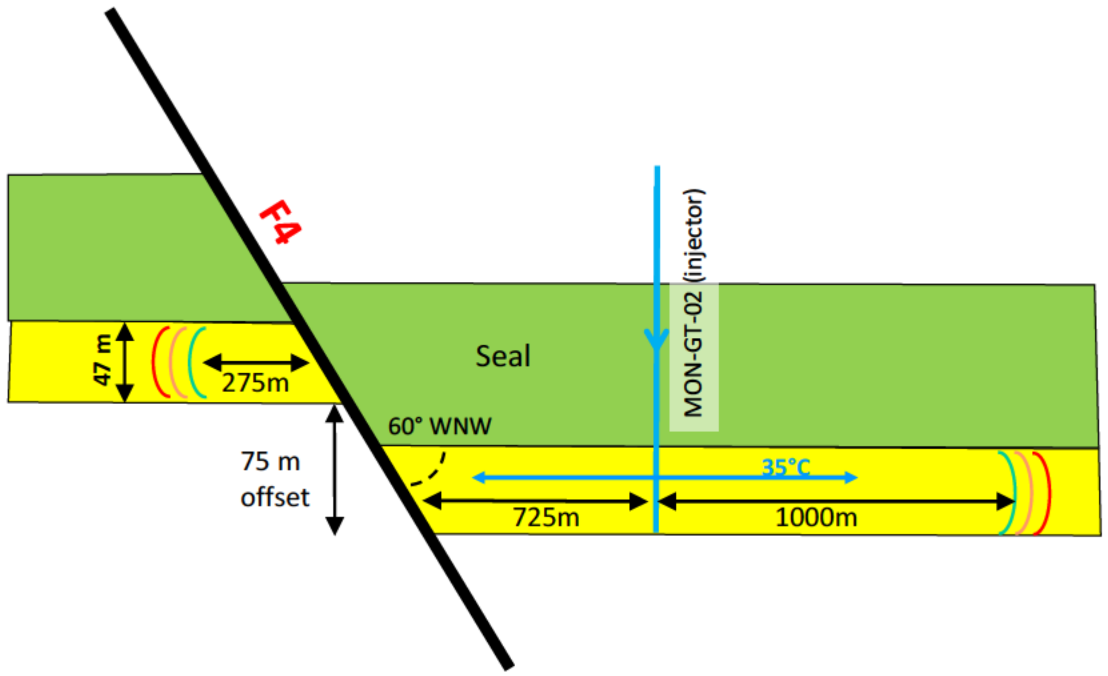

Figure 5-20 MON-GT-02 Delft F4: Side view (cross section) of injector, the fault and computed extent of the cooled zone at the end of field life.

5.2.1 0 years of injection (before start of injection).

5.2.1.1 Deterministic analysis

To start with, a fault stability analysis prior to injection was carried out with the objective to have a "reference case" of stability with which the impact of different injection can be compared. As is well-known, the "reference case"-situation can have an important impact on the feasibility of a geothermal project. For example, if in the reference case, the shear stress on the fault is already close to its maximum allowable value for fault reactivation, cold water injection will be not or hardly feasible. An well-known example of such a situation in The Netherlands is Limburg.

Figure 5-21 shows the situation and corresponding SCU for the Polanen case. As can be seen, the pre-injection SCU of the fault is equal to approximately 0.55 for the base case parameter values.

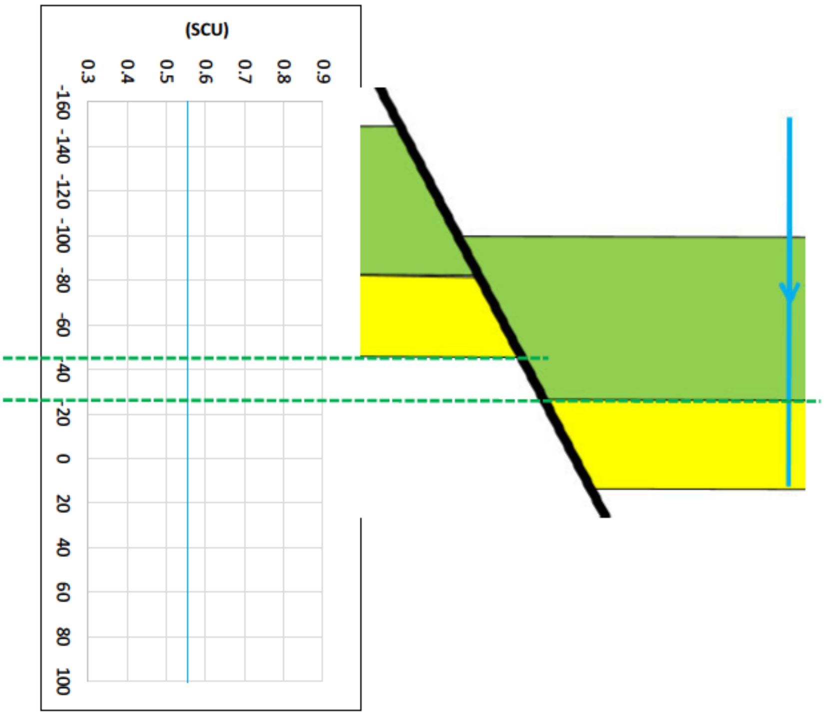

Figure 5-21 MON-GT-02 0 years, Delft F4: Computed SCU along the fault at the before start of injection.

5.2.1.2 Probabilistic analysis (Monte Carlo)

In order to address the impact of parameter uncertainties, a Mohr-Coulomb Monte-Carlo analysis was carried out using an ensemble of 1000 members. The addressed uncertain parameters are shown in Table 5-3, which displays the input parameters for the probabilistic analysis of the Delft formation and the F4 fault, including their low-med-high values. The parameters and reasoning have been discussed in section 3.3. Because for zero injection, the injector distance to the fault is irrelevant, and therefore this uncertainty has not been included in the current analysis (indicated by strikethrough in the table).

Table 5-3 Input parameters for probabilistic analysis of the Delft formation and the F4 Fault. See text for discussion.

	Parameter	Min	Median	Max
Rock Parameters	Reservoir Temperature (°C)	83	86	89
	Thermoelastic coefficient (bar/°C)	0.5	1.0	1.5
	Vertical stress gradient (bar/m)	0.21	0.22	0.23
	Horizontal stress gradient (bar/m)	0.144	0.158	0.189
Fault Parameters	Cohesion (bar)	0	15	30
	Friction coefficient (-)	0.48	0.60	0.72
	Dip (degrees)	50	60	70
	~~Distance from injector (m)~~	~~625~~	~~725~~	~~825~~

The results of this analysis are shown in Figure 5-22 and Figure 5-23. The majority of SCU values seen are in the 0.4-0.7 range, with 1.6% having an SCU between 0.9 and 1 (based on the P90 Mohr-Coulomb failure line), and 0.2% an SCU > 1 (based on the P90 Mohr-Coulomb failure line).

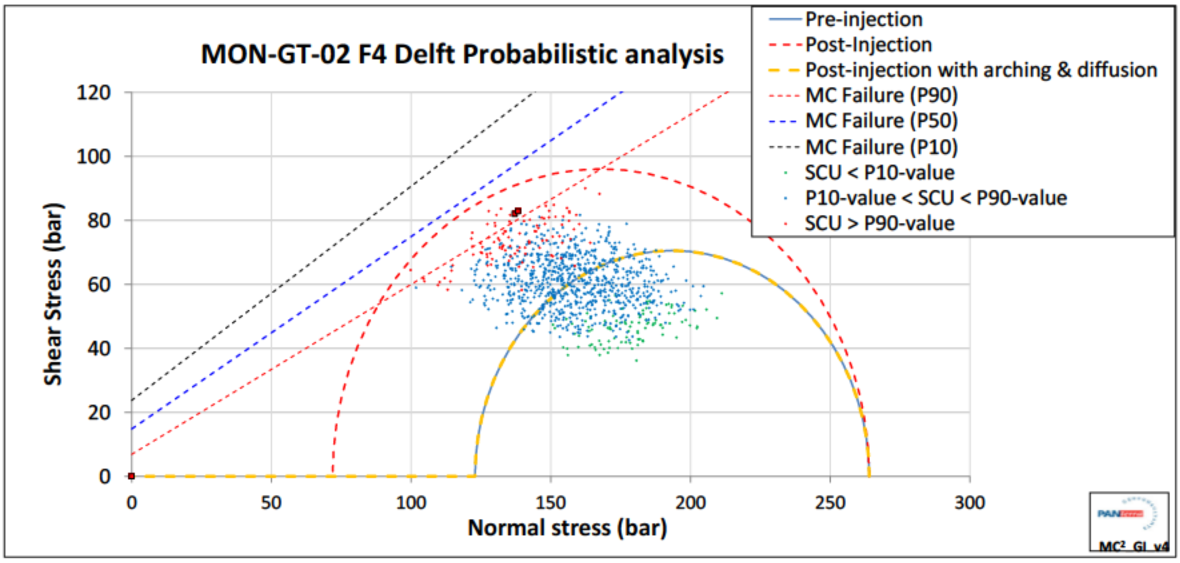

Figure 5-22 Results of Mohr-Coulomb Monte-Carlo for the F4 fault prior to injection into MON-GT-02. The dots represent the simulations, colours indicating the P10,P50 and P90 results. Three reference Mohr Circles are presented based on the median input: initial state (blue solid circle), result assuming full reservoir cooling (red-dashed circle) and result including arching & temperature diffusion (orange-dashed circle). Please note that in this case, the blue and orange-dashed circles coincide because no cold water has been injected (yet).

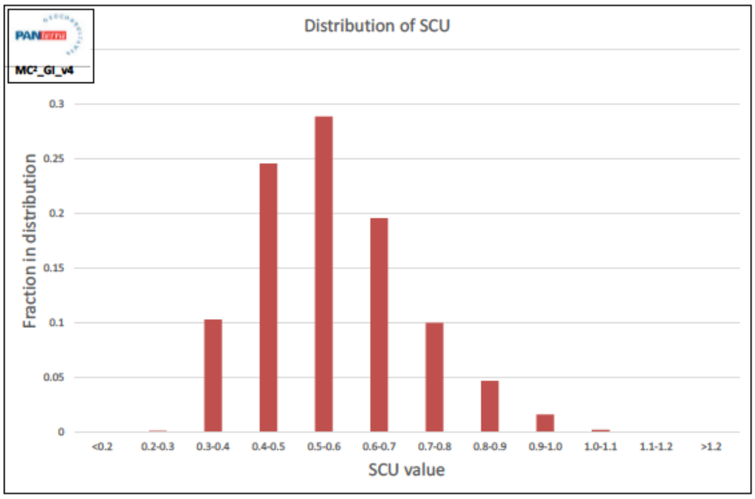

Figure 5-23 Probability diagram of the simulated SCU values prior to injection. The bulk of the values are 0.4 and 0.7, with 1.6% between 0.9 and 1 (based on the P90 Mohr-Coulomb failure line), and 0.2% with SCU > 1.0 (based on the P90 Mohr-Coulomb failure line).

5.2.2 10 years of injection

5.2.2.1 Temperature profile

The computed temperature profile away from the injector after 10 years of injection is presented in Figure 5-24. The cooled zone is not an abrupt front but rather influenced by thermal diffusion, both within the reservoir and from the cap- and baserock into the reservoir.

After 10 years of injection we observe a temperature alteration up to 600 m. This is considered the cold water "front". The F4 fault is expected at 725 m. This scenario is schematically depicted in Figure 5-24.

Based on the seismic, the fault offset has been estimated at 75 m.

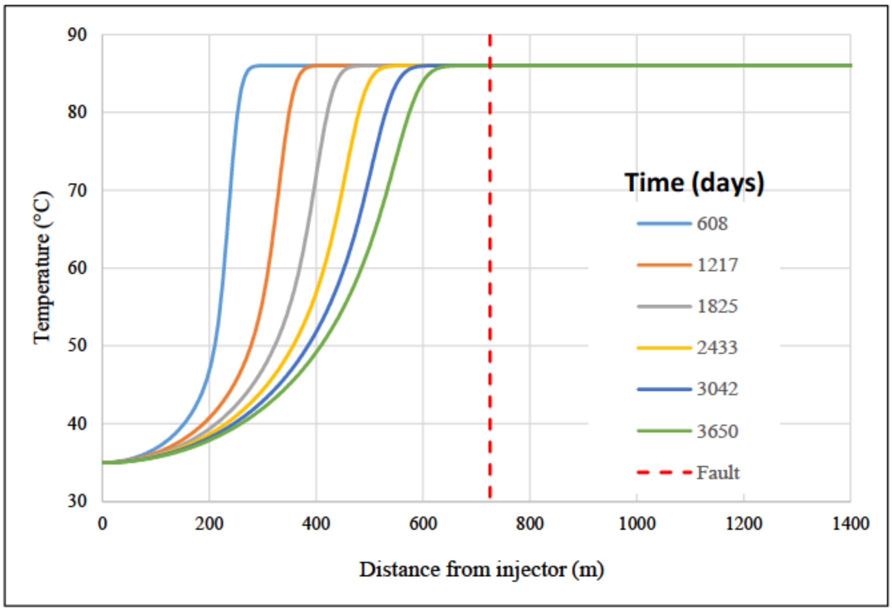

Figure 5-24 Temperature profile in the reservoir away from the injector after 10 years of injection.

5.2.2.2 Deterministic analysis

The methodology as described in Section 3.1 is applied to estimate the impact of the cooling on the Shear Capacity Utilisation (SCU). In order to take into account the effect of partial cooling, the entire temperature profile in the cooled zones to the left and to the right of the fault is computed. Subsequently, the thermo-elastic stress change on the fault resulting from this temperature profile is calculated. As a fault position is a matter of interpretation and faults often display 'damage zones' an uncertainty was taken into account in the fault position of ±100 m.

The results are given in Figure 5-25 where the SCU is calculated for the initial state as well as the state of fault affected by a nearby cooled area. This shows the computed SCU along the fault after 10 years of injection. As can be seen, the maximum SCU is around 0.61 which is still significantly below 1. Varying the fault distance over ±100 m with respect to base case of 725 m from injector results in an SCU-variation between 0.57 and 0.61.

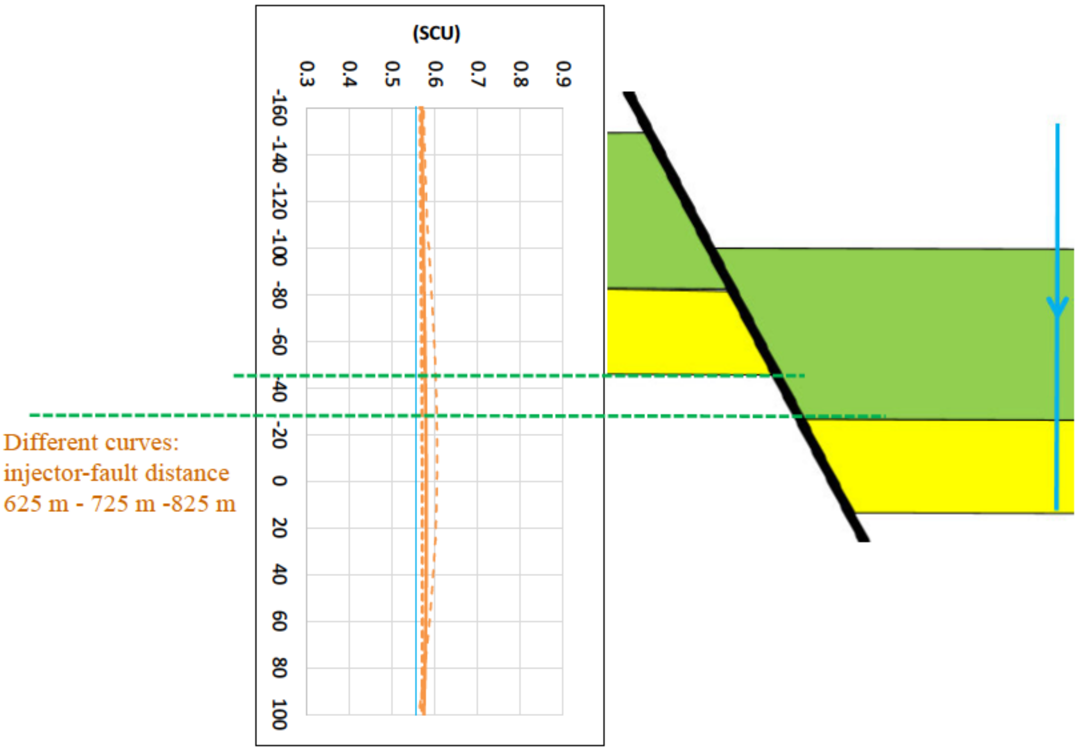

Figure 5-25 Computed SCU along the fault after 10 years of injection. The "worst point" is addressed in a Monte-Carlo simulation. Dashed lines indicate the results based on a fault uncertainty of ±100m.

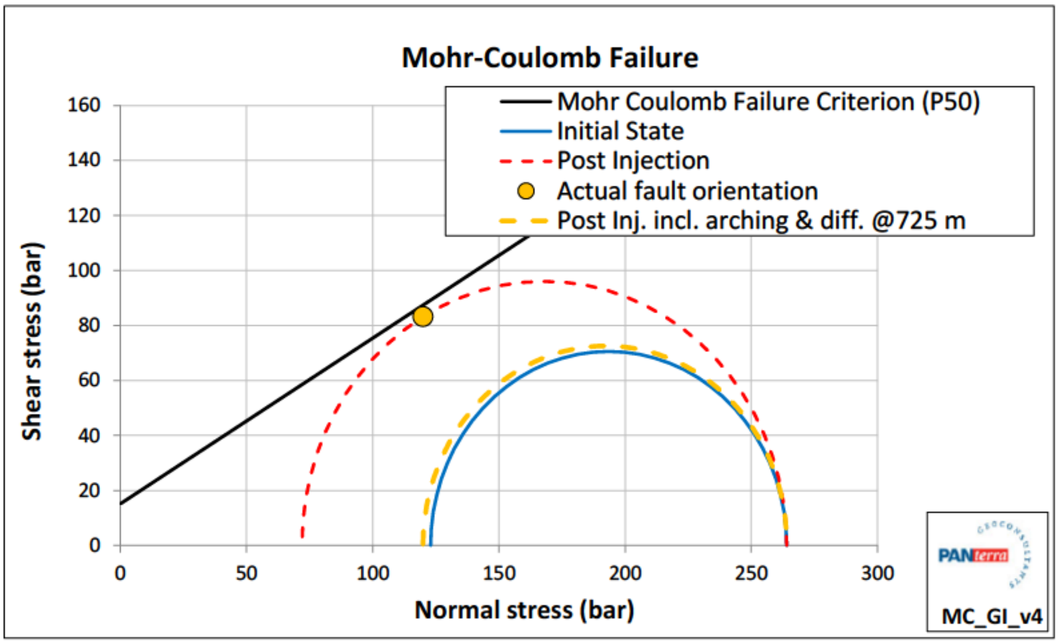

Figure 5-26 Mohr circles after 10 years of injection for the Delft formation at the "worst" point along the fault (see fig. 5-25).

Figure 5-26 shows a deterministic failure analysis for the "worst" point on the SCU curve of Figure 5-25. This figure shows the Mohr circles at the beginning of field life and after 10 years of injection for the base case scenario of a transmissible fault at 725 m. The red dashed Mohr circle is obtained by assuming a uniform cooling down to the injection temperature of 35°C across the entire reservoir. The yellow dashed Mohr circle includes the actual change of state of stress as a result of the cooled area, i.e. it includes the

impact of stress arching by uncooled areas further away from the injector. Also, the approach presented here includes the impact of stress concentrations along the fault.

It should be noted that the impact of stress arching is very high in this case (Figure 5-26). For this particular case, the result can be explained by the fact that the cold front has not yet crossed the fault. As will be shown below, with progressing injection, the degree of stress arching decreases, in line with expectations.

5.2.2.3 Probabilistic analysis (Monte Carlo)

In order to address the impact of parameter uncertainties, a Mohr-Coulomb Monte-Carlo analysis was carried out using an ensemble of 1000 members. The addressed uncertain parameters are shown in Table 5-4, which displays the input parameters for the probabilistic analysis of the Delft formation and the F4 fault, including their low-med-high values. The parameters and reasoning have been discussed in section 4.3.

The results of this analysis are shown in Figure 5-27 and Figure 5-28. The Mohr circles shown are the same as those in Figure 5-26. The majority of SCU values seen are in the 0.4-0.7 range, with 1.5% having an SCU between 0.9 and 1 (based on the P90 Mohr-Coulomb failure line), and 0.3% an SCU > 1 (based on the P90 Mohr-Coulomb failure line). Please note that these results are identical to the case of 0 years injection.

In conclusion, after 10 years of injection, the likelihood of activation of the F4 fault by injecting 35°C water into the Delft formation via MON-GT-02 can be considered negligible.

Table 5-4 Input parameters for probabilistic analysis of the Delft formation and the F4 Fault.

	Parameter	Min	Median	Max
Rock Parameters	Reservoir Temperature (°C)	83	86	89
	Thermoelastic coefficient (bar/°C)	0.5	1.0	1.5
	Vertical stress gradient (bar/m)	0.21	0.22	0.23
	Horizontal stress gradient (bar/m)	0.144	0.158	0.189
Fault Parameters	Cohesion (bar)	0	15	30
	Friction coefficient (-)	0.48	0.60	0.72
	Dip (degrees)	50	60	70
	Distance from injector (m)	625	725	825

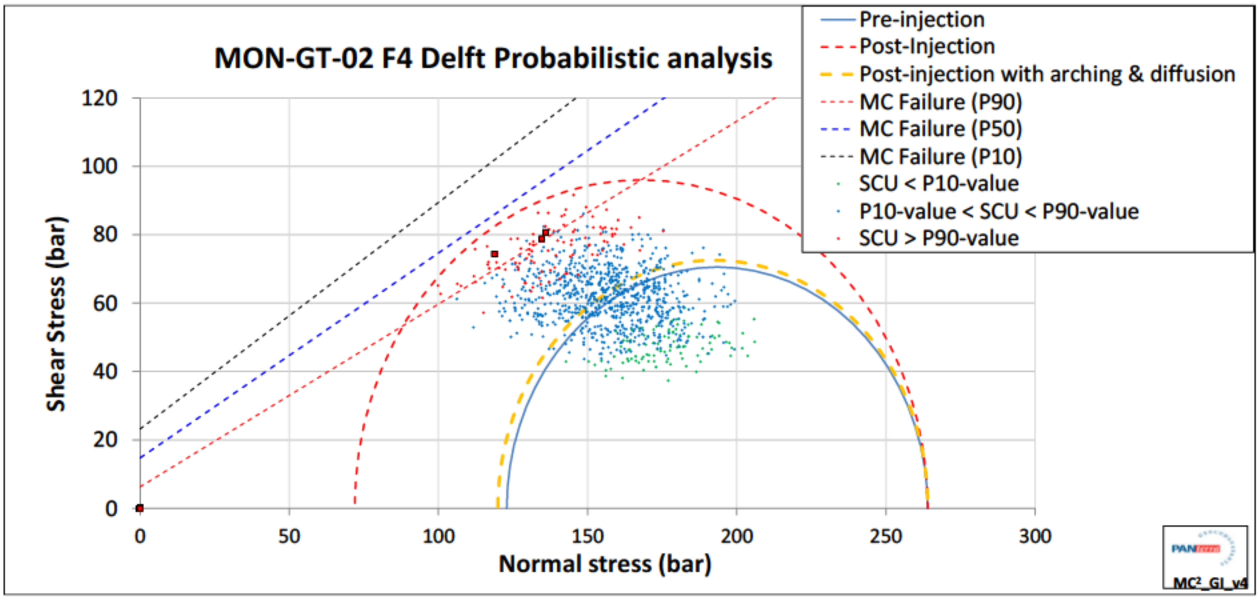

Figure 5-27 Results of Mohr-Coulomb Monte-Carlo for cooling around the F3 fault as a result of doublet MON-GT-02, after 10 years of injection The dots represent the simulations, colours indicating the P10,P50 and P90 results. Three reference Mohr Circles are presented based on the median input: initial state (blue solid circle), result assuming full reservoir cooling (red-dashed circle) and result including arching & temperature diffusion (orange-dashed circle).

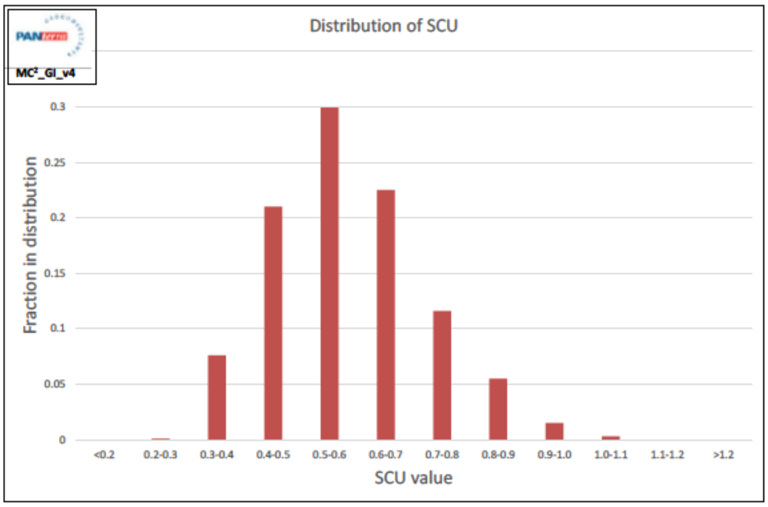

Figure 5-28 Probability diagram of the simulated SCU values after 10 years of injection. The bulk of the values are in between 0.4 and 0.8, with 1.5% between 0.9 and 1 (based on the P90 Mohr-Coulomb failure line), and 0.3% with SCU > 1.0 (based on the P90 Mohr-Coulomb failure line).

5.2.3 20 years of injection

5.2.3.1 Temperature profile

The computed temperature profile away from the injector after 20 years of injection is presented in Figure 5-29. The cooled zone is not an abrupt front but rather influenced by thermal diffusion, both within the reservoir and from the cap- and baserock into the reservoir. After 20 years of injection we observe a temperature alteration up to 850 m.

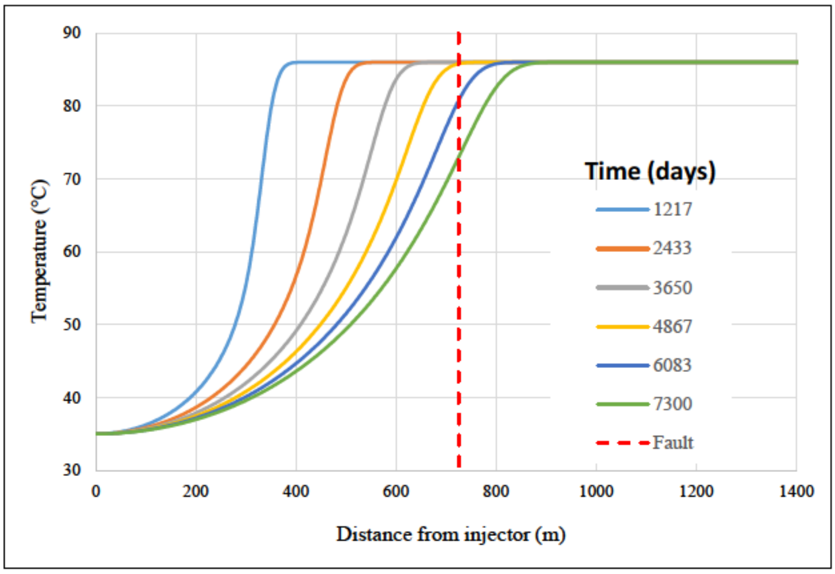

Figure 5-29 Temperature profile in the reservoir away from the injector after 20 years of injection.

5.2.3.2 Deterministic analysis

The results are given in Figure 5-30 where the SCU is calculated for the initial state as well as the state of fault affected by a nearby cooled area. This shows the computed SCU along the fault after 20 years of injection. As can be seen, the maximum SCU (e.g. at vertical coordinate $x \approx -20$ m) is around 0.77 which is still significantly below 1. Varying the fault distance over ±100 m with respect to base case of 725 m from injector results in an SCU-variation between 0.60 and 0.77.

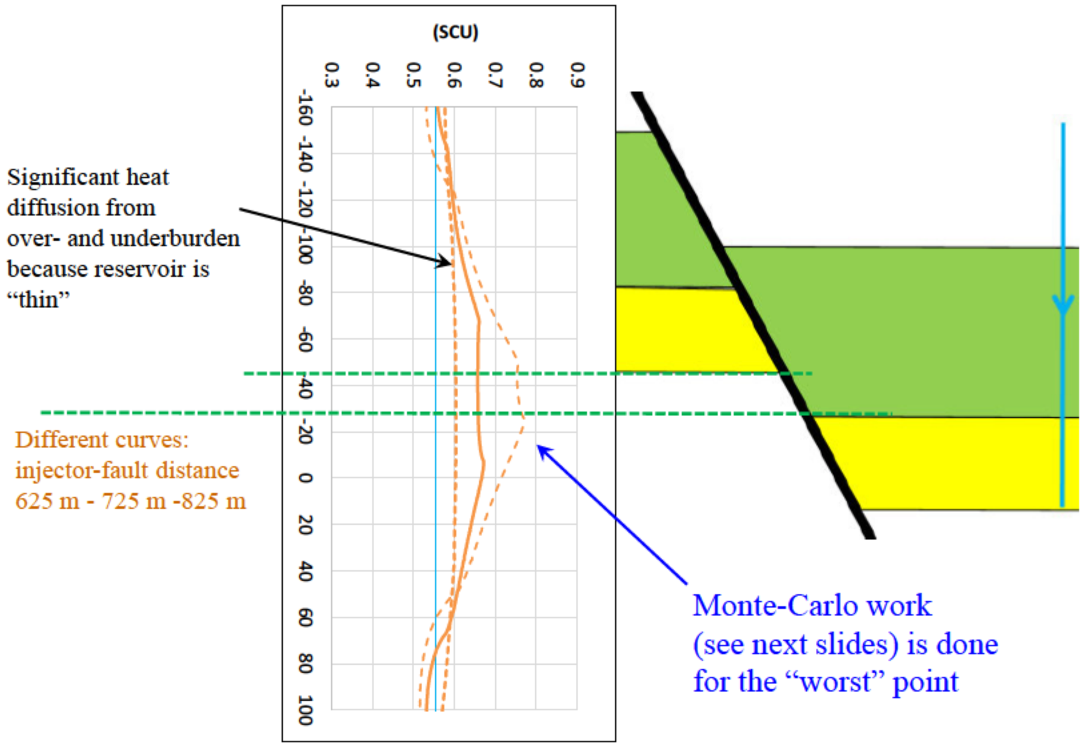

Figure 5-30 Computed SCU along the fault after 20 years of injection. The "worst point" is addressed in a Monte-Carlo simulation. Dashed lines indicate the results based on a fault uncertainty of ±100m.

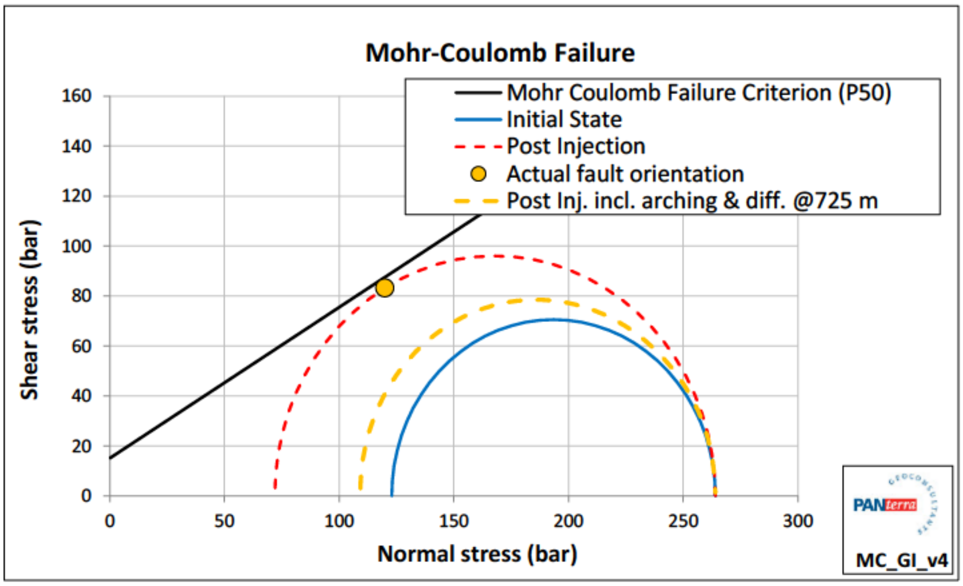

Figure 5-31 Mohr circles after 20 years of injection for the Delft formation at the "worst" point along the fault (see fig. 5-30).

Figure 5-31 shows a deterministic failure analysis for the "worst" point on the SCU curve of Figure 5-30. This figure shows the Mohr circles at the beginning of field life and after 20 years of injection for the base case scenario of a transmissible fault at 725 m. The red dashed Mohr circle is obtained by assuming a uniform cooling down to the injection temperature of 35°C across the entire reservoir. The yellow dashed Mohr circle includes the actual change of state of stress as a result of the cooled area, i.e. it includes the

impact of stress arching by uncooled areas further away from the injector. Also, the approach presented here includes the impact of stress concentrations along the fault.

It should be noted that the impact of stress arching is still reasonably pronounced in this case (Figure 5-31), though less than after 10 years of injection (Figure 5-26). This can be explained by the fact that the cooled zone has crossed the fault, but its lateral extent is not (yet) very large compared to the reservoir thickness.

5.2.3.3 Probabilistic analysis (Monte Carlo)

In order to address the impact of parameter uncertainties, a Mohr-Coulomb Monte-Carlo analysis was carried out using an ensemble of 1000 members. The addressed uncertain parameters are shown in Table 5-4 above.

The results of this analysis are shown in Figure 5-32 and Figure 5-33. The Mohr circles shown are the same as those in Figure 5-31. The majority of SCU values seen are in the 0.5-0.8 range, with 8% having an SCU between 0.9 and 1 (based on the P90 Mohr-Coulomb failure line), and 3% an SCU > 1 (based on the P90 Mohr-Coulomb failure line).

In conclusion, after 20 years of injection, the likelihood of activation of the F4 fault by injecting 35°C water into the Delft formation via MON-GT-02 can no longer be considered very small.

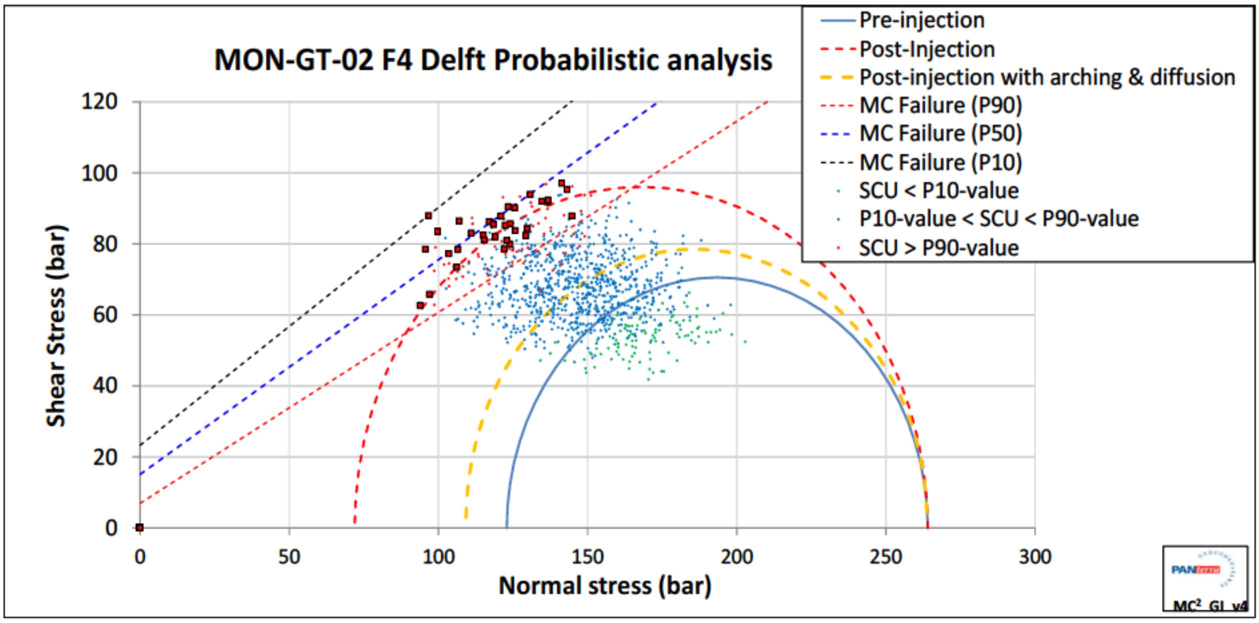

Figure 5-32 Results of Mohr-Coulomb Monte-Carlo for cooling around the F4 fault as a result of doublet MON-GT-02, after 20 years of injection The dots represent the simulations, colours indicating the P10,P50 and P90 results. Three reference Mohr Circles are presented based on the median input: initial state (blue solid circle), result assuming full reservoir cooling (red-dashed circle) and result including arching & temperature diffusion (orange-dashed circle).

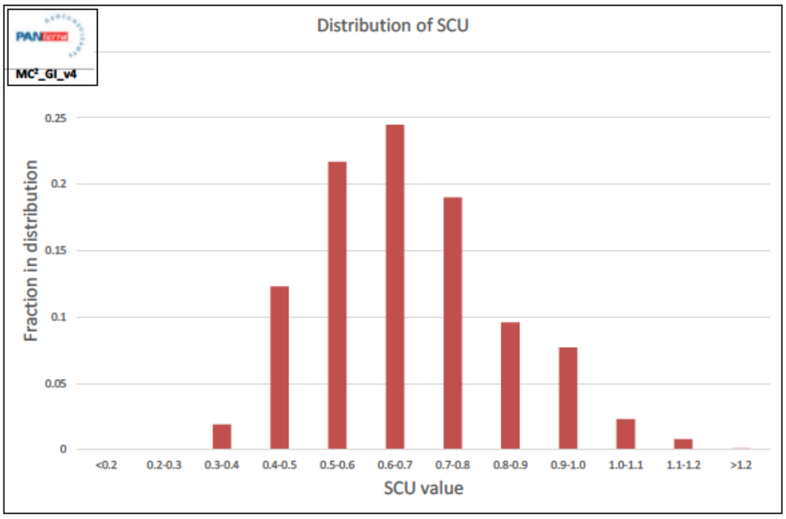

Figure 5-33 Probability diagram of the simulated SCU values after 20 years of injection. The bulk of the values are in between 0.5 and 0.8, with 8% between 0.9 and 1 (based on the P90 Mohr-Coulomb failure line), and 3% with SCU > 1.0 (based on the P90 Mohr-Coulomb failure line).

5.2.4 30 years of injection

5.2.4.1 Temperature profile

The computed temperature profile away from the injector after 30 years of injection is presented in Figure 5-34. The cooled zone is not an abrupt front but rather influenced by thermal diffusion, both within the reservoir and from the cap- and baserock into the reservoir. After 30 years of injection we observe a temperature alteration up to 1000 m.

5.2.4.2 Deterministic analysis

The results are given in Figure 5-35 where the SCU is calculated for the initial state as well as the state of fault affected by a nearby cooled area. This shows the computed SCU along the fault at the end of field life (30 years of injection). As can be seen, the maximum SCU (e.g. at vertical coordinate x ≈ -30 m) is around 0.83 which is still well below 1. Varying the fault distance over ±100 m with respect to base case of 625 m from injector results in an SCU-variation between 0.68 and 0.83.

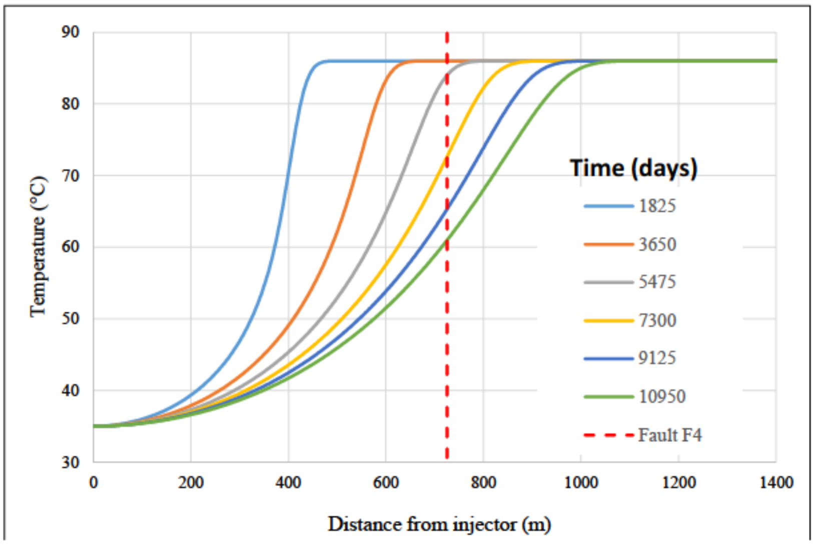

Figure 5-34 Temperature profile in the reservoir away from the injector after 30 years of injection.

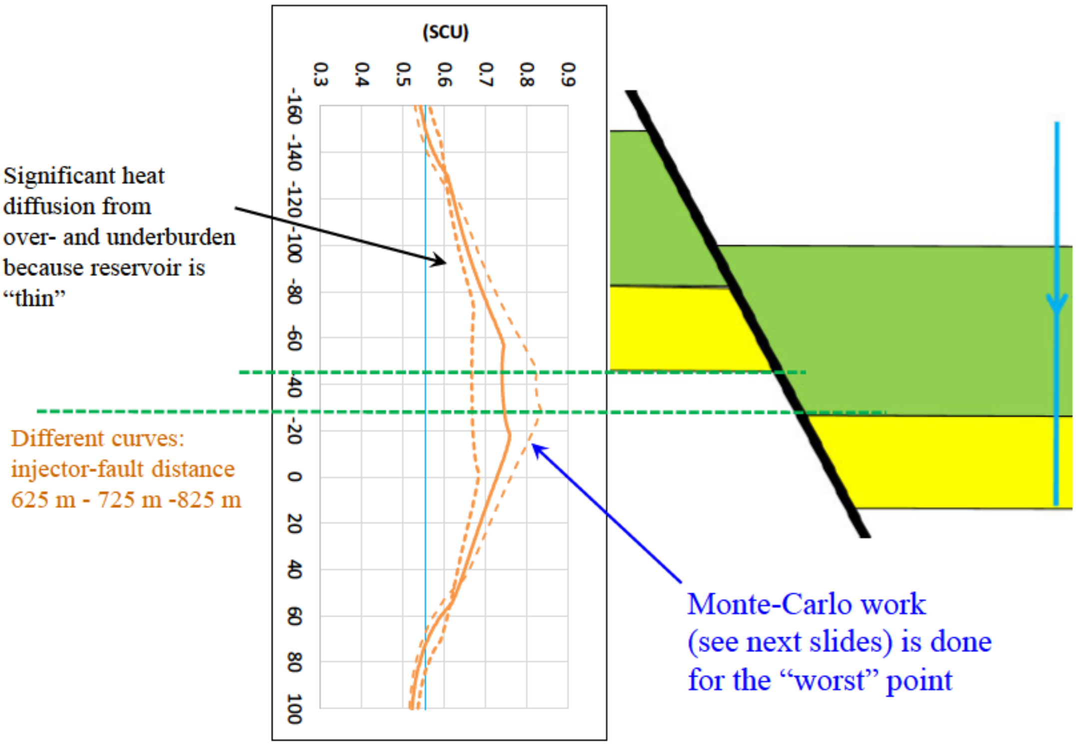

Figure 5-35 Computed SCU along the fault after 30 years of injection. The "worst point" is addressed in a Monte-Carlo simulation. Dashed lines indicate the results based on a fault uncertainty of ±100m.

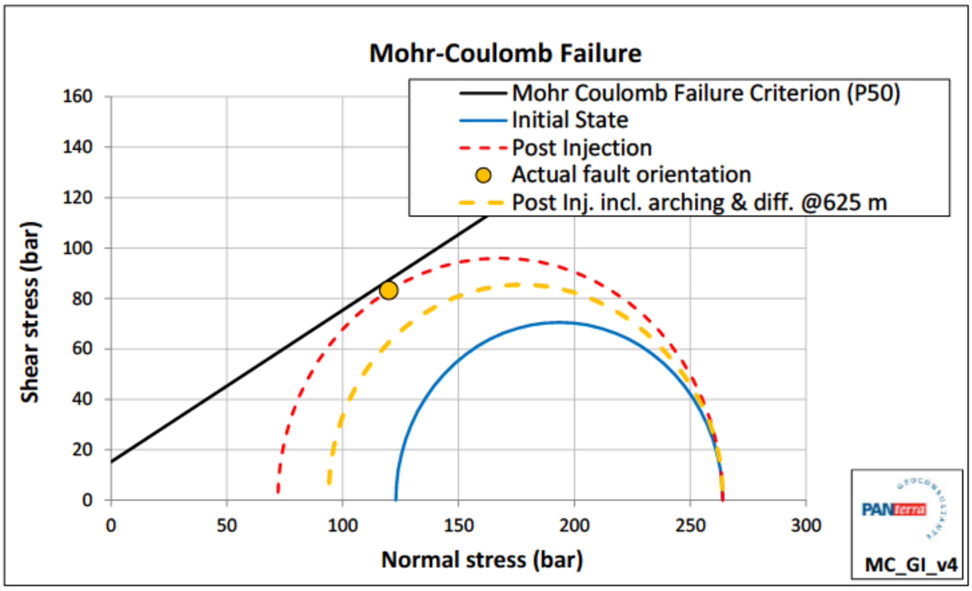

Figure 5-36 Mohr circles after 30 years of injection for the Delft formation at the "worst" point along the fault (see fig. 5-35).

Figure 5-36 shows a deterministic failure analysis for the "worst" point on the SCU curve of Figure 5-35. This figure shows the Mohr circles at the beginning of field life and after 30 years of injection for the base case scenario of a transmissible fault at 725 m. The red dashed Mohr circle is obtained by assuming a uniform cooling down to the injection temperature of 35°C across the entire reservoir. The yellow dashed Mohr circle includes the actual change of state of stress as a result of the cooled area, i.e. it includes the

impact of stress arching by uncooled areas further away from the injector. Also, the approach presented here includes the impact of stress concentrations along the fault.

It should be noted that the impact of stress arching is still present in this case (Figure 5-36), though clearly less than after 10 and 20 years of injection (Figure 5-26 and Figure 5-31). This can be explained by the fact that the lateral extent of the cooled zone around the fault is starting to grow large compared to the reservoir thickness.

5.2.4.3 Probabilistic analysis (Monte Carlo)

In order to address the impact of parameter uncertainties, a Mohr-Coulomb Monte-Carlo analysis was carried out using an ensemble of 1000 members. The addressed uncertain parameters are shown in Table 5-4 above.

The results of this analysis are shown in Figure 5-37 and Figure 5-38. The Mohr circles shown are the same as those in Figure 5-36. The majority of SCU values seen are in the 0.5-1.0 range, with 12% having an SCU between 0.9 and 1 (based on the P90 Mohr-Coulomb failure line), and 10% an SCU > 1 (based on the P90 Mohr-Coulomb failure line).

In conclusion, after 30 years of injection, the likelihood of activation of the F4 fault by injecting 35°C water into the Delft formation via MON-GT-02 can be considered non-negligible.

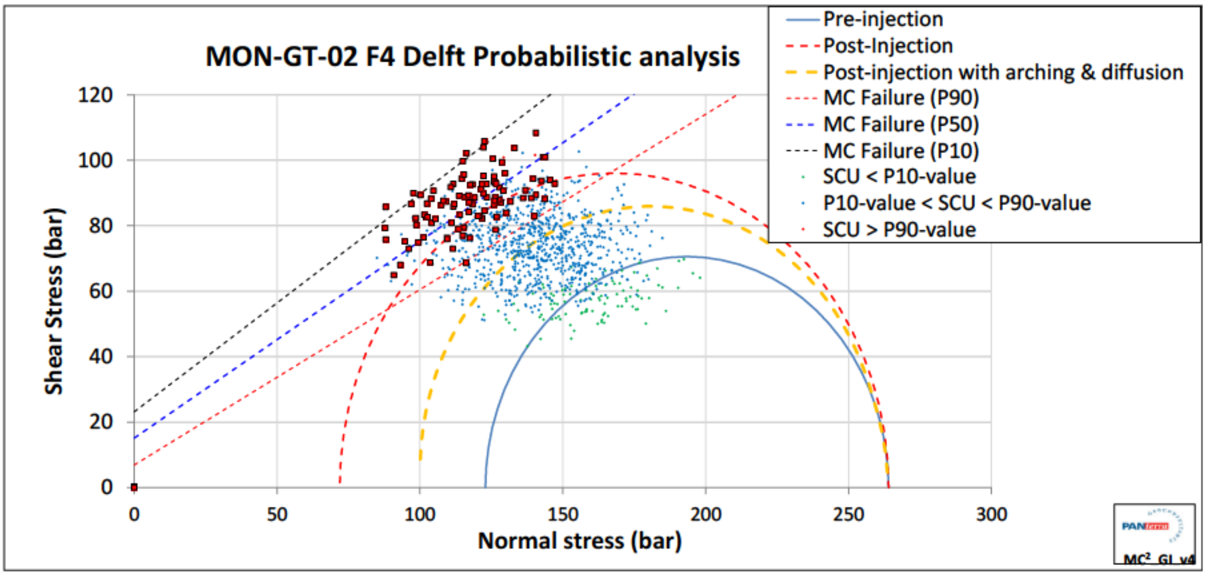

Figure 5-37 Results of Mohr-Coulomb Monte-Carlo for cooling around the F4 fault as a result of doublet MON-GT-02, after 30 years of injection The dots represent the simulations, colours indicating the P10,P50 and P90 results. Three reference Mohr Circles are presented based on the median input: initial state (blue solid circle), result assuming full reservoir cooling (red-dashed circle) and result including arching & temperature diffusion (orange-dashed circle).

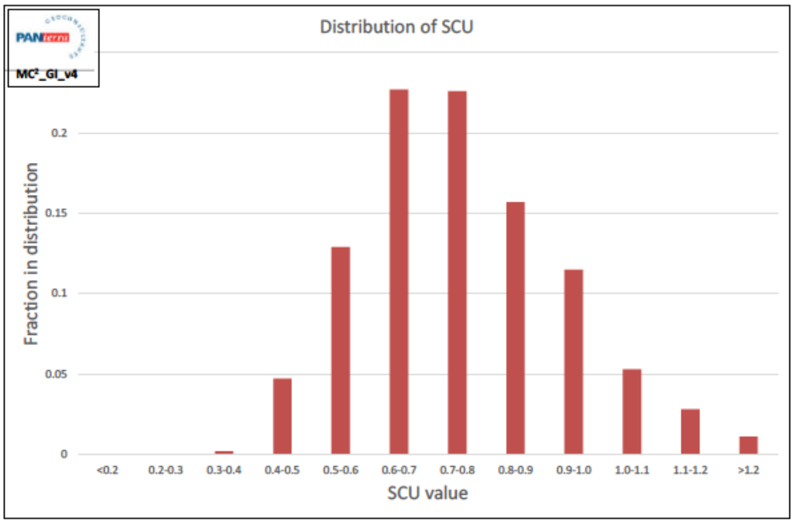

Figure 5-38 Probability diagram of the simulated SCU values after 30 years of injection. The bulk of the values are in between 0.5 and 1.0, with 12% between 0.9 and 1 (based on the P90 Mohr-Coulomb failure line), and 10% with SCU > 1.0 (based on the P90 Mohr-Coulomb failure line).

6 Conclusions

This report presents a level-2 SHA study for Polanen. A conservative approach was applied for all cases in the sense that it was assumed that faults are non-sealing. As a result, a maximum size of the cooled zones on either side of the fault was achieved in the study, thus leading to minimal scope for arching by adjacent uncooled zones.

The results can be summarised as follows:

- For both faults F3 and F4, the risk of fault reactivation as a result of the geothermal operation is small for the first ~ 15 years because the cold front has not yet reached the fault.
- For t > 15 years, this risk slowly increases as a result of the fact that the cold front crosses the fault and cools part of the reservoir at the opposite side. Eventually, at the end of field life (after 30 years of injection), about 10% of the cases in the Monte Carlo analysis result in an SCU exceeding one.

7 References

Buijze, L., van den Bogert, P. A. J., Wassing, B. B. T., Orlic, B., & ten Veen, J. (2017). Fault reactivation mechanisms and dynamic rupture modelling of depletion-induced seismic events in a Rotliegend gas reservoir. *Netherlands Journal of Geosciences*, *96*(5), s131–s148. https://doi.org/10.1017/njg.2017.27

de Jager, J., Doyle, M. A., Grantham, P. J., & Mabillard, J. E. (1996). Hydrocarbon habitat of the West Netherlands Basin. In H. E. Rondeel, D. A. J. Batjes, & W. H. Nieuwenhuijs (Eds.), *Geology of Gas and Oil under the Netherlands* (pp. 191–209). Springer Netherlands. https://doi.org/10.1007/978-94-009-0121-6_17

Duin, E. J. T., Doornenbal, J. C., Rijkers, R. H. B., Verbeek, J. W., & Wong, Th. E. (2006). Subsurface structure of the Netherlands—Results of recent onshore and offshore mapping. *Netherlands Journal of Geosciences - Geologie En Mijnbouw*, *85*(4), 245–276. https://doi.org/10.1017/S0016774600023064

Hunfeld, L. B., Niemeijer, A. R., & Spiers, C. J. (2017). Frictional Properties of Simulated Fault Gouges from the Seismogenic Groningen Gas Field Under In Situ *P* - *T* -Chemical Conditions: Friction of Groningen fault gouges. *Journal of Geophysical Research: Solid Earth*, *122*(11), 8969–8989. https://doi.org/10.1002/2017JB014876

Koning, E. J. L. (1988). *Waterflooding under fracturing conditions*. http://citeseerx.ist.psu.edu/viewdoc/download?doi=10.1.1.913.17&rep=rep1&type=pdf

PanTerra. (2018). *Geological study of the subsurface of Polanen, G1421*.

PanTerra. (2020a). *Polanen Seismic Interpretation 3D Depth survey R-2629,1900011*.

PanTerra. (2020b). *Seismic Hazard Analysis—Level 1 (Quick-Scan) Polanen*.

Perkins, T. K., & Gonzalez, J. A. (1985). The Effect of Thermoelastic Stresses on Injection Well Fracturing. *Society of Petroleum Engineers Journal*, *25*(01), 78–88. https://doi.org/10.2118/11332-PA

Poessé, J. W., & van den Hoek, P. (2020). Semi-Quantitative Assessment of Seismic Hazard in Geothermal Reservoirs. *Day 1 Tue, December 01, 2020*, D011S004R003. https://doi.org/10.2118/200544-MS

Q-CON/IF technology. (2016). *Defining the Framework for Seismic Hazard Assessment in Geothermal Projects V0.1*. https://www.kasalsenergiebron.nl/content/user_upload/Kennisagenda_-_Defining_framework_for_Seismic_Hazard_Assessment_in_Geothermal_Projects_-_Technical_Report_-_161005.pdf

Samuelson, J., & Spiers, C. J. (2012). Fault friction and slip stability not affected by Co2 storage: Evidence from short-term laboratory experiments on North Sea reservoir sandstones and caprocks. *International Journal of Greenhouse Gas Control*, *11*, S78–S90. https://doi.org/10.1016/j.ijggc.2012.09.018

Santarelli, F. J., Havmoller, O., & Naumann, M. (2008). Geomechanical Aspects of 15 Years Water Injection on a Field Complex: An Analysis of the Past to Plan the Future. *All Days*, SPE-112944-MS. https://doi.org/10.2118/112944-MS

Stevens, D. G., Murray, L. R., & Shah, P. C. (2000). Predicting Multiple Thermal Fractures in Horizontal Injection Wells; Coupling of a Wellbore and a Reservoir Simulator. *All Days*, SPE-59354-MS. https://doi.org/10.2118/59354-MS

Svendsen, A. P., Wright, M. S., Clifford, P. J., & Berry, P. J. (1991). Thermally Induced Fracturing off Ula Water Injectors. *SPE Production Engineering*, *6*(04), 384–390. https://doi.org/10.2118/20898-PA

TNO. (2014). *DoubletCalc 1.4 manual*. TNO. https://www.nlog.nl/sites/default/files/6ab98fc3-1ca1-4bbe-b0a2-c5a9658a3597_doubletcalc%20v143%20manual.pdf

van den Bogert, P. (2015). *Impact of various modelling options on the onset of fault slip and the fault slip reponse using 2-dimensional Finite- Element modelling.* https://www.researchgate.net/publication/348785769_Impact_of_various_modelling_options_on_the_onset_of_fault_slip_and_the_fault_slip_reponse_using_2-dimensional_Finite-_Element_modelling van den Hoek, P. J., & Poessé, J. W. (2021). Assessment of Seismic Risk in Geothermal and Hydrocarbon Reservoirs Using an Exact Analytical Solution of Stress Change. *Day 3 Wed, October 20, 2021*, D031S007R002. https://doi.org/10.2118/205122-MS

Verweij, J. M., Simmelink, H. J., Underschultz, J., & Witmans, N. (2012). Pressure and fluid dynamic characterisation of the Dutch subsurface. *Netherlands Journal of Geosciences - Geologie En Mijnbouw*, *91*(4), 465–490. https://doi.org/10.1017/S0016774600000342